AGU PUBLICATIONS

Paleoceanography

RESEARCH ARTICLE
10.1002/2014PA002658

Key Points:
- As proxy of past ocean circulation changes, eps(Nd) has strong potential
- Simultaneously occurring MOC anomalies compromise reconstructions
- Atlantic paleorecords of eps(Nd) indicative of AMOC strengthening during T1

Supporting Information:
- Table S1

Correspondence to:
T. Friedrich,
tobiasf@hawaii.edu

Citation:
Friedrich, T., A. Timmermann, T. Stichel, and K. Pahnke (2014), Ocean circulation reconstructions from ϵ_{Nd}: A model-based feasibility study, *Paleoceanography*, *29*, 1003–1023, doi:10.1002/2014PA002658.

Received 11 APR 2014
Accepted 29 SEP 2014
Accepted article online 2 OCT 2014
Published online 4 NOV 2014

Ocean circulation reconstructions from ϵ_{Nd}: A model-based feasibility study

T. Friedrich[1], A. Timmermann[1], T. Stichel[2], and K. Pahnke[3]

[1]International Pacific Research Center, School of Ocean and Earth Sciences and Technology, University of Hawaii at Manoa, Honolulu, Hawaii, USA, [2]Ocean and Earth Science, National Oceanography Centre Southampton, University of Southampton, Southampton, UK, [3]Institute for Chemistry and Biology of the Marine Environment, Carl von Ossietzky University, Oldenburg, Germany

Abstract Over the past decade, records of the seawater neodymium isotopic composition (ϵ_{Nd}) have become a widely used proxy to reconstruct changes in ocean circulation. Our study investigates the transient response of ϵ_{Nd} to large-scale ocean circulation changes using an Earth system model of intermediate complexity. It is shown that a weakening of the North Atlantic Deep Water formation results in positive ϵ_{Nd} anomalies in the Atlantic and the Pacific below 1000 m water depth whereas variations in Antarctic Bottom Water production generate a Pacific-Atlantic dipole pattern of deep ocean ϵ_{Nd} changes. Further experiments explore which ocean regions are suitable to record the temporal evolution of the overturning in the North Atlantic and the Southern Ocean by means of ϵ_{Nd} data. High local correlations occur between simulated Southern Ocean overturning changes and simulated ϵ_{Nd} anomalies in the deep North Pacific and almost globally for simulated North Atlantic overturning changes, respectively, clearly indicating the strong potential of ϵ_{Nd} to work as a proxy of past ocean circulation changes. Finally, the compromising effects of simultaneously occurring anomalies in the North Atlantic and the Southern Ocean overturning cells on reconstructions of past ocean circulation changes are identified. Combining our model simulations with currently available core data, our study demonstrates that changes in ϵ_{Nd} documented in numerous Atlantic paleorecords clearly support the notion of a strengthening in the Atlantic Meridional Overturning Circulation over the course of Termination 1.

1. Introduction

Climate variability over the last glacial cycles has been closely linked to large-scale ocean circulation changes. To reconstruct past ocean circulation variability, various proxies have been used, such as Pa/Th [e.g., *Hoffmann et al.*, 2013; *Lippold et al.*, 2012; *McManus et al.*, 2004; *Negre et al.*, 2010; *Burke et al.*, 2011; *Marchal et al.*, 2000; *Yu et al.*, 1996], benthic $\delta^{13}C$ [e.g., *Pahnke and Zahn*, 2005; *Curry and Oppo*, 2005; *Hesse et al.*, 2011] and $\Delta^{14}C$ [e.g., *Okazaki et al.*, 2010; *Skinner et al.*, 2010; *Butzin et al.*, 2005]. In the last decade, a growing number of studies have relied on records of the isotopic composition of neodymium (Nd) to draw conclusions about past ocean circulation changes [*Rutberg et al.*, 2000; *Piotrowski et al.*, 2004; *Foster et al.*, 2007; *Gutjahr et al.*, 2008; *Piotrowski et al.*, 2008; *Pahnke et al.*, 2008; *Robinson and van de Flierdt*, 2009; *Piotrowski et al.*, 2009; *Colin et al.*, 2010; *Gutjahr et al.*, 2010; *Horikawa et al.*, 2010; *Roberts et al.*, 2010; *Crocket et al.*, 2011; *Gutjahr and Lippold*, 2011; *Xie et al.*, 2012; *Piotrowski et al.*, 2012; *Pena et al.*, 2013; *Noble et al.*, 2013].

Neodymium is a rare Earth element with seven naturally occurring isotopes. The five isotopes ^{142}Nd, ^{143}Nd, ^{145}Nd, ^{146}Nd, and ^{148}Nd are stable. ^{144}Nd and ^{150}Nd are radioactive isotopes. However, their half-life times are estimated to be in the order of 10^{15} and 10^{19} years, respectively. Thus, they can be regarded as stable for the timescales considered here.

The Nd isotopic composition (ϵ_{Nd}) is expressed in the ϵ-notation defined as

$$\epsilon_{Nd} = \left(\frac{(^{143}Nd/^{144}Nd)_{sample}}{(^{143}Nd/^{144}Nd)_{CHUR}} - 1 \right) \times 10^4 \quad (1)$$

where CHUR represents the present-day Chondritic Uniform Reservoir, which amounts to 0.512638 [*Jacobsen and Wasserburg*, 1980]. The radiogenic isotope ^{143}Nd is the decay product of ^{147}Sm, which is why

©2014. American Geophysical Union. All Rights Reserved.

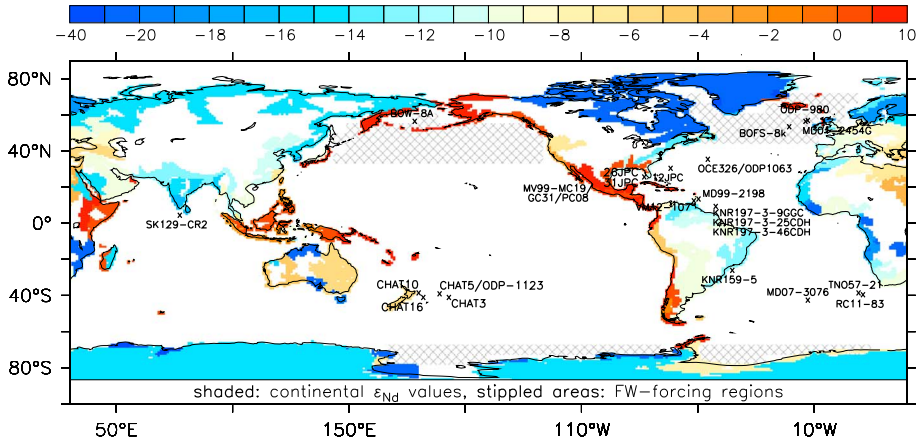

Figure 1. Shaded: Continental values of ϵ_{Nd} [*Jeandel et al.*, 2007; *Roy et al.*, 2007] used for relaxation at the continental boundaries of the ocean model between 0 and 3000 m. Locations of currently available ϵ_{Nd} data with a focus on the Last Glacial Termination are indicated by crosses. Please see also Table 1 for details regarding the cores. Stippled areas indicate regions of freshwater (FW) forcing for the different experiments. See also Table 2 for experiment details.

the ϵ_{Nd} is a function of the Sm/Nd ratio which in turn is higher in the Earth's mantle compared to its crust. As a consequence, the Nd isotopic composition of the continents is subject to a heterogeneous distribution [*Goldstein and Hemming*, 2003; *Jeandel et al.*, 2007] (see Figure 1). The mainly young, mantle-derived rocks surrounding the Pacific are found to have high ϵ_{Nd} values, whereas the age of the rocks that encompasses the North Atlantic is in the order of 10^9 years resulting in lower isotopic ratios [*Frank*, 2002].

The change in ϵ_{Nd} of seawater at the ocean margins is thought to be largely determined by local weathering inputs from rivers and by exchange with the sediment—referred to as "boundary exchange" (BE) [*Lacan and Jeandel*, 2005]—leaving an imprint of the regional ϵ_{Nd} signature on the water mass. In the ocean interior, ϵ_{Nd} exhibits a quasi-conservative behavior hence bearing the potential to operate as a tracer of ocean circulation and mixing [*Piepgras and Wasserburg*, 1982; *von Blanckenburg*, 1999; *Goldstein and Hemming*, 2003]. Nd isotopes are incorporated into Fe-Mn coatings at the seafloor. Thus, these precipitates can preserve the isotopic composition of the water mass directly overlying the sediment and can potentially provide insights into the state of the ocean circulation at the time of formation. (Please refer to *Tachikawa et al.* [2014] for a detailed review.)

Substantial effort has been undertaken to model the cycling of Nd and ϵ_{Nd} in the ocean. The complexity of the approaches runs the gamut from box models [*Bertram and Elderfield*, 1993] to simplify modeling simulations of the ϵ_{Nd} cycle in ocean general circulation models of different resolution [*Arsouze et al.*, 2007, 2008, 2010; *Jones et al.*, 2008] to sophisticated studies of both Nd concentrations and ϵ_{Nd} [*Siddall et al.*, 2008; *Arsouze et al.*, 2009; *Rempfer et al.*, 2011].

The study by *Rempfer et al.* [2012a] was the first to investigate the relationship between ϵ_{Nd} and changes in the overturning circulation in idealized model experiments. They showed that ϵ_{Nd} variations occur in response to simulated millennial-scale changes in overturning and found the largest simulated ϵ_{Nd} variations in regions where the contribution of water masses depends on the circulation regime. The study also documented that the sign of simulated ϵ_{Nd} anomalies in the deep Atlantic and Pacific differs between overturning changes in the North Atlantic and the Southern Ocean which facilitates discrimination between the two overturning cells in case ϵ_{Nd} records from the deep Atlantic and Pacific are available. Overall, *Rempfer et al.* [2012a] demonstrated the large potential of ϵ_{Nd} as an indicator of past ocean circulation and its limitation for quantitative reconstructions of MOC changes.

Our study builds on the results of *Rempfer et al.* [2012a] by showing the fingerprints of large-scale MOC changes in a three-dimensional Earth system model. In addition, we are exploring which ocean seafloor regions are promising to record and reconstruct meridional overturning changes occurring in the North Atlantic and the Southern Ocean. The possibility to reconstruct ocean circulation changes during the Last Glacial Termination from currently available ϵ_{Nd} data is investigated using two different nonparametric

©2014. American Geophysical Union. All Rights Reserved.

Table 1. Name, Location, Depth, and Reference for ϵ_{Nd} Cores Used in This Study[a]

Core Name	Location	Depth	Reference	Panel
		North Atlantic		
ODP-980	55.4833°N / 14.7000°W	2168 m	*Crocket et al.* [2011]	m
MD01-2454G	55.5193°N / 15.6513°W	747 m	*Colin et al.* [2010]	c
BOFS 8K	52.5000°N / 22.1000°W	4045 m	*Piotrowski et al.* [2012]	n
OCE326-GGC6	33.6907°N / 57.5760°W	4541 m	*Roberts et al.* [2010]	r
ODP-1063	33.6833°N / 57.6167°W	4584 m	*Gutjahr and Lippold* [2011]	s
12JPC	29.0747°N / 72.8983°W	4250 m	*Gutjahr et al.* [2008]	o
KNR166-2-26JPC	24.3270°N / 83.2523°W	546 m	*Xie et al.* [2012]	d
KNR166-2-31JPC	24.2197°N / 83.2958°W	751 m	*Xie et al.* [2012]	e
MD99-2198	12.1500°N / 61.3833°W	1330 m	*Pahnke et al.* [2008]	h
VM12-107	11.3300°N / 66.6300°W	1079 m	*Xie et al.* [2014]	i
KNR197-3-25GGC	7.7045°N / 53.7853°W	671 m	*Huang et al.* [2014]	j
KNR197-3-46CDH	7.8360°N / 53.6633°W	947 m	*Huang et al.* [2014]	j
KNR197-3-9GGC	7.9300°N / 53.5752°W	1100 m	*Huang et al.* [2014]	j
		South Atlantic		
KNR159-5-36GGC	27.8500°S / 46.7833°W	1268 m	*Pahnke et al.* [2008]	g
RC11-83	41.0700°S / 9.7170°E	4718 m	*Rutberg et al.* [2000] *Piotrowski et al.* [2004] *Piotrowski et al.* [2005] *Piotrowski et al.* [2008]	q
TNO57-21	40.1300°S / 7.8200°E	4981 m	*Piotrowski et al.* [2005] *Piotrowski et al.* [2008]	l
MD07-3076	44.0743°S / 14.2078°W	3770 m	*Skinner et al.* [2013]	i
		North Pacific		
BOW-8A	54.7833°N / 176.9167°E	884 m	*Horikawa et al.* [2010]	a
MV99-MC19/ GC31/PC08	23.5000°N / 111.6000°W	705 m	*Basak et al.* [2010]	f
		South Pacific		
ODP-1123	41.7860°S / 171.4990°W	3290 m	*Elderfield et al.* [2012]	p
CHAT 3K	42.6600°S / 167.5000°W	4,802 m	*Noble et al.* [2013]	k
CHAT 5K	40.7800°S / 171.5500°W	4240 m	*Noble et al.* [2013]	k
CHAT 10K	40.0300°S / 180.0000°W	3003 m	*Noble et al.* [2013]	k
CHAT 16K	42.5333°S / 178.4983°W	1408 m	*Noble et al.* [2013]	k
		Indian Ocean		
SK129CR2	3.0000°N / 76.0000°E	3800 m	*Piotrowski et al.* [2009]	b

[a]Letter in the right column indicates the panel in which temporal evolution of core data are shown by Figure 2. See also Figure 1 for core locations. ODP, Ocean Drilling Program.

regression techniques. Furthermore, we demonstrate the deteriorating effects of simultaneously occurring changes in North Atlantic and Southern Ocean overturning on the interpretation of ϵ_{Nd} records. Finally, the shared variability of a compilation of currently available ϵ_{Nd} records from the Atlantic during Termination 1 is analyzed with regard to the changes in the simulated North Atlantic overturning circulation in our idealized model experiments.

Our paper is organized as follows: Section 2 provides an overview of the currently available ϵ_{Nd} records that cover the Last Glacial Termination. The configuration of the Earth system model is explained in section 3 and in the supporting information. Detailed descriptions of the ϵ_{Nd} modeling and the experiment design are given in sections 4 and 5, respectively. Our results are presented and discussed in section 6, and a summary is given in section 7.

2. ϵ_{Nd} Data for Termination I

The paleo ϵ_{Nd} data sets used in the present study were selected based on the following criteria: (1) coverage of the Last Glacial Termination or parts of it and (2) a sufficient temporal resolution. The locations of 26 cores were investigated with regard to their potential to record overturning changes through ϵ_{Nd} anomalies in the ambient water. Eleven cores were selected from the North Atlantic [*Colin et al.*, 2010; *Crocket et al.*, 2011;

©2014. American Geophysical Union. All Rights Reserved.

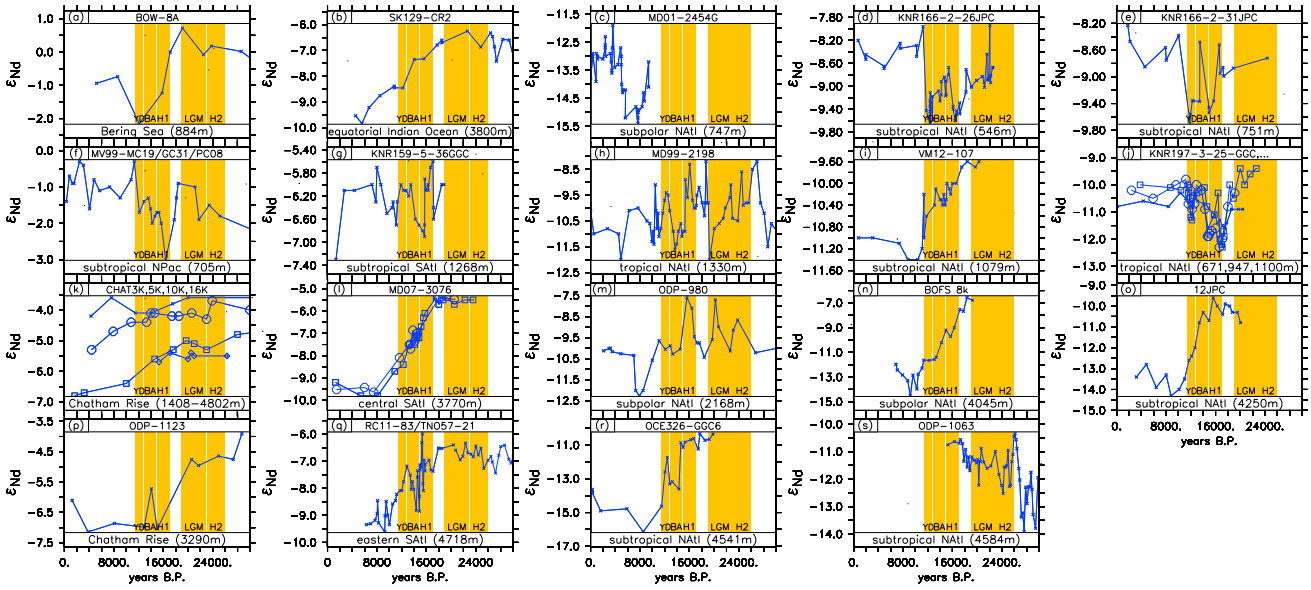

Figure 2. Currently available ϵ_{Nd} data with focus on the Last Glacial Termination. Please see Table 1 for details regarding the cores and Figure 1 for core locations.

Gutjahr et al., 2008; *Gutjahr and Lippold*, 2011; *Pahnke et al.*, 2008; *Roberts et al.*, 2010; *Xie et al.*, 2012; *Piotrowski et al.*, 2012; *Xie et al.*, 2014; *Huang et al.*, 2014], four from the South Atlantic [*Rutberg et al.*, 2000; *Piotrowski et al.*, 2004, 2005, 2008; *Pahnke et al.*, 2008; *Skinner et al.*, 2013] . Two cores are located in the North Pacific [*Horikawa et al.*, 2010; *Basak et al.*, 2010]. One core is located in the Northern Indian Ocean [*Piotrowski et al.*, 2009], and five cores stem from the Chatham Rise in the Southern Ocean [*Elderfield et al.*, 2012; *Noble et al.*, 2013]. Figure 1 depicts the core locations. The cores cover depths ranging from 546 m to 4981 m. Table 1 provides an overview of the core locations and references. The temporal evolution of the ϵ_{Nd} data across Termination I is presented in Figure 2.

3. Model Configuration

To study the response of ϵ_{Nd} to changes in ocean circulation, we conducted a series of idealized freshwater perturbation experiments under preindustrial climate conditions using the atmosphere-ocean-sea ice-carbon cycle model LOVECLIM [*Goosse et al.*, 2010]. LOVECLIM is based on the ECBilt-CLIO Earth system model of intermediate complexity extended by vegetation and marine carbon cycle components. A more detailed model description can be found in the supporting information.

An additional passive tracer was initialized in order to study the effects of large-scale changes in ocean circulation on the distribution of ϵ_{Nd}. Subsequently, freshwater forcing was applied over different regions to induce changes in the different meridional overturning circulation cells. Details on the configurations and the experiment designs are given in the following two sections.

4. Simulation of the Neodymium Isotopic Composition

The Nd isotopic composition of seawater is mainly determined by the exchange at the continental margins, input through rivers and dust, and an internal cycling caused by adsorption of and desorption from sinking particles (reversible scavenging). A recent modeling study by *Rempfer et al.* [2011] revealed that the boundary exchange (BE) between seawater and the continental margins represents the major source (~90%) of Nd, whereas riverine and dust input are important in the upper 500 m. With regard to the effect on the Nd isotopic composition of seawater, *Rempfer et al.* [2012b] stated that variations in ϵ_{Nd} resulting from changes in dust or river input are relatively small and largely constrained to the upper 1000 m of the water column. In our study, we chose to solely simulate the variations in ϵ_{Nd} and not the actual cycling of Nd isotopes mainly to reduce the computational effort. In our simplified approach, only BE of ϵ_{Nd} is taken into account following the approach of *Arsouze et al.* [2007]. ϵ_{Nd} is implemented as a passive tracer which is subject to the exact

©2014. American Geophysical Union. All Rights Reserved.

same advection and mixing as, e.g., temperature and salinity. The BE is parametrized through a relaxation at the continental margins of the ocean model at depths between 0 and 3000 m:

$$\Delta\epsilon_{Nd} = \frac{1}{\tau(z)} \cdot (\text{mask}^{\epsilon_{Nd}} - \epsilon_{Nd}) \quad (2)$$

$$\frac{\partial\epsilon_{Nd}}{\partial t} = \Delta\epsilon_{Nd} + \text{advection} + \text{mixing} \quad (3)$$

The relaxation values at the continental margins ($\text{mask}^{\epsilon_{Nd}}$, Figure 1) follow data of *Jeandel et al.* [2007] (with updated values for Antarctica by *Roy et al.* [2007]) which have been interpolated onto the grid of the ocean model around its continental margins for depths of 0–3000 m. The relaxation timescale $\tau(z)$ increases exponentially with depth [*Arsouze et al.*, 2007, 2008]

$$\tau(z) = 0.5 \cdot e^{\frac{z[\text{m}]}{500\ \text{m}}}\ [\text{years}] \quad (4)$$

The above equation results in relaxation timescales of $\tau(0\ \text{m}) = 0.5$ years; $\tau(1500\ \text{m}) \simeq 10$ years and $\tau(3000\ \text{m}) \simeq 200$ years, respectively. The concept of a depth-dependent relaxation timescale is motivated by the different magnitudes of current velocities at different depths with higher velocities providing more energy for sediment-seawater interactions. It must be noted, however, that a recent study reported a boundary exchange influence at 4000 m along the Madagascar and Mascarene margins [*Wilson et al.*, 2012]. Furthermore, uncertainty is introduced by the fact that the boundary exchange kinetics are most likely also governed by the type of source rock. For instance, *Wilson et al.* [2013] reported that a volcanic component in sediments contributes preferentially to the BE of ϵ_{Nd}. Therefore, the BE may be subject to large geographic variability. Given the lack of global data of BE rates, we pursue the more idealized approach described by equation (3).

The effect of reversible scavenging on the local ϵ_{Nd} composition of seawater is neglected in our parametrization. Due to the fact that ^{143}Nd and ^{144}Nd are isotopes of the same element with virtually identical masses, no isotopic fractionation occurs during the processes of adsorption onto sinking particles and desorption during dissolution. However, reversible scavenging represents a vertical piggyback transport of ϵ_{Nd} as near surface ϵ_{Nd} values are exported to the deep through sinking particles. The latter can cause an offset of ϵ_{Nd} values compared to other water mass tracers such as salinity (see Figure 10 in *Rempfer et al.* [2011]).

Whereas reversible scavenging is one important component to explain the vertical distribution of Nd, the contribution of different particle types and adsorption coefficients remains highly elusive [*Siddall et al.*, 2008]. Furthermore, it is unclear to what degree reversible scavenging affects the ϵ_{Nd} distribution. On the one hand, modeling studies demonstrated a dependency of ϵ_{Nd} on the parametrization of reversible scavenging [*Arsouze et al.*, 2009; *Siddall et al.*, 2008; *Rempfer et al.*, 2011]. On the other hand, observational studies concluded that the behavior of ϵ_{Nd} can be regarded as "quasi-conservative" [*Piepgras and Wasserburg*, 1982; *von Blanckenburg*, 1999; *Goldstein and Hemming*, 2003].

In our control simulation, the ϵ_{Nd} tracer is initialized with a value of zero in the entire model domain of the ocean component of the LOVECLIM model. The Earth system model is then integrated under preindustrial boundary conditions (except for the closed Bering Strait) using the described relaxation scheme. After 4000 years the ϵ_{Nd} tracer is equilibrated in all ocean basins. Figure 3 shows a validation of simulated ϵ_{Nd} values against the global compilation of seawater ϵ_{Nd} [*Lacan et al.*, 2012]. The model is capable of reproducing the large-scale features of ϵ_{Nd} with positive (negative) end-member values in the North Atlantic (North Pacific). The lowest values of ϵ_{Nd} are found near the production regions of North Atlantic Deep Water (NADW). In agreement with the observations, ϵ_{Nd} clearly increases along the path of the NADW in our simulation (not shown). High-simulated ϵ_{Nd} values are present at the continental margins in the North Pacific. In the North Pacific and in particular in the North Atlantic simulated ϵ_{Nd} values exhibit a larger scatter than the observations (Figure 3a, black and red crosses). We speculate that in case of the North Atlantic the substantial deviations are at least partly caused by the strong spatial gradient in ϵ_{Nd} that exist between Greenland/Scandinavia and Iceland (Figure 1). The relatively coarse resolution of the model does not allow for a reliable representation of features associated with a strong spatial ϵ_{Nd} gradient. With respect to the North Pacific we suppose that the lack of reversible scavenging in the parametrization of the seawater ϵ_{Nd} may lead to a slightly overestimated vertical ϵ_{Nd} gradient compared to the observations.

©2014. American Geophysical Union. All Rights Reserved.

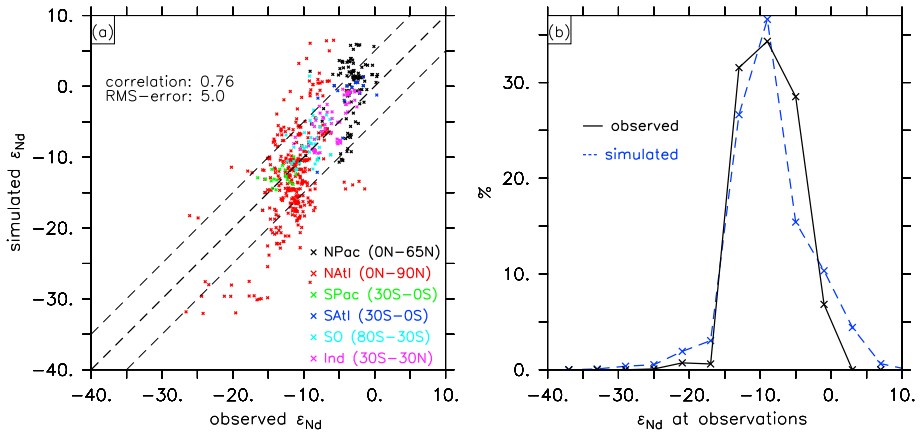

Figure 3. (a) Observed [*Lacan et al.*, 2012] and simulated ϵ_{Nd}. Colors indicate different ocean basins provided in the panel. The point-to-point correlation is 0.76. The RMS-error amounts to 5.0. (b) Distribution of simulated (dashed blue line) and observed (solid black line) ϵ_{Nd} (bin size: 5).

In the South Atlantic, the South Pacific, the Southern Ocean, and the Indian Ocean ϵ_{Nd} observations are well captured by the model simulation. Overall, the point-to-point pattern correlation between the observations [*Lacan et al.*, 2012] and the simulated values at the corresponding model grid cells is 0.76 (Figure 3a), and the distributions of simulated and observed ϵ_{Nd} are in good agreement (Figure 3b) which provides further confidence in our simplified approach.

In this study we employ a simplified parametrization of seawater ϵ_{Nd} that is admittedly subject to numerous shortcomings and caveats as outlined above. However, we chose to only simulate ϵ_{Nd} instead of the actual Nd isotopes.

As much as a more elaborated parametrization that includes the cycling of the actual Nd isotopes would be desirable, it should be noted that the latter is also subject to large uncertainties arising mainly from the sources of Nd and insufficiently constrained coefficients that enter the governing equations (see *Rempfer et al.* [2011] for a detailed discussion).

In addition, the focus of our manuscript is the transient response of seawater ϵ_{Nd} to large-scale reorganizations in ocean circulation (see next section for experiment design). It needs to be kept in mind that these changes are associated with large-scale changes in, e.g., wind fields, precipitation patterns, sea surface temperature, and nutrient availability. These changes are believed to have largely altered dust input [*Moreno et al.*, 2002; *Itambi et al.*, 2009; *Kienast et al.*, 2013], river runoff [*Tjallingii et al.*, 2008], and marine primary production [*Thomas et al.*, 1995; *Kienast et al.*, 2006; *Menviel et al.*, 2008] making it even more difficult to validate the numerous assumptions regarding dust and river input of Nd as well as the adsorption and desorption of Nd on particle surfaces that more complex parametrizations are partly based on.

Finally, it should be noted that the overall model performance in particular with respect to the representation of ocean currents and water mass distribution will have a strong effect on the reproduction of ϵ_{Nd} observations. Mismatches in the ϵ_{Nd} simulation can originate from an insufficient parametrization of the ϵ_{Nd} or Nd cycle as well as from biases in the modeled ocean circulation which affects the distribution of simulated water masses and thus the one of simulated ϵ_{Nd}. Hence, one has to be cautious with the adjustment of parameters of the ϵ_{Nd} or Nd cycle as it bears the risk of tuning the ϵ_{Nd} or Nd parametrization to, e.g., insufficient model physics.

5. Experiment Design

A series of experiments is conducted to study the transient response of ϵ_{Nd} to large-scale ocean circulation changes and to test the usefulness of ϵ_{Nd} as a water mass tracer. Ocean circulation changes were induced by freshwater (FW) forcing in different ocean regions indicated by the stippled areas in Figure 1. The FW forcing was applied over ocean grid points only and without the use of salt compensation as the latter leads to artifacts in the ocean circulation response [*Stocker et al.*, 2007]. The FW forcing used in the simulations is

©2014. American Geophysical Union. All Rights Reserved.

Table 2. Abbreviations and Descriptions of the Model Experiments and Locations and Strength of the Freshwater (FW) Forcing[a]

Model Run	Description	FW-Forcing Region	FW-Forcing Details
AMOC−	simulation of a Heinrich event	North Atlantic	constant 2000 years 0.5 Sv
AMOC+	simulation of an AMOC strengthening	North Atlantic	constant 2000 years −0.5 Sv
PMOC+	simulation of a NPac MOC strengthening	North Pacific	constant 2000 years −0.35 Sv
SOMOC−	simulation of a Southern Ocean MOC shutdown	Ross Sea and Weddell Sea	constant 1000 years 0.2 Sv
SOMOC+	simulation of a Southern Ocean MOC strengthening	Ross Sea and Weddell Sea	constant 1000 years −0.2 Sv
AMOC$\pm^m$ (millennial scale)	alternating AMOC strengthening and weakening	North Atlantic	alternating ±0.5 Sv for 2000 years
SOMOC$\pm^m$ (millennial scale)	alternating Southern Ocean MOC strengthening and weakening	Ross Sea and Weddell Sea	alternating ±0.2 Sv for 2000 years
AMOC$\pm^c$ (centennial scale)	alternating AMOC strengthening and weakening	North Atlantic	alternating ±0.5 Sv for 200 years
SOMOC$\pm^c$ (centennial scale)	alternating Southern Ocean MOC strengthening and weakening	Ross Sea and Weddell Sea	alternating ±0.2 Sv for 200 years
MIXVAR1	simultaneous AMOC + SOMOC strengthening and weakening	North Atlantic, Ross Sea and Weddell Sea	alternating combination of AMOC$\pm^m$ and SOMOC$\pm^c$
MIXVAR2	simultaneous AMOC + SOMOC strengthening and weakening	North Atlantic, Ross Sea and Weddell Sea	alternating combination of AMOC$\pm^c$ and SOMOC$\pm^m$

[a]A negative FW forcing indicates FW extraction from the surface. See stippled areas in Figure 1 for FW-forcing regions. The temporal evolutions of the FW forcing and the overturning indices are shown in Figure 4. AMOC, Atlantic Meridional Overturning Circulation; SOMOC, Southern Ocean Meridional Overturning; MOC, Meridional Overturning Circulation; PMOC, Pacific Meridional Overturning Circulation. Sv, sverdrup (10^6 m^3/s).

highly idealized and oriented on the sensitivity of the Earth system model. It is not intended to represent reconstructed changes in past sea level.

In total we conducted 11 model experiments. There are five baseline simulations using constant FW forcing in a single ocean basin: *AMOC*−, *AMOC*+, *PMOC*+, *SOMOC*−, and *SOMOC*+. Furthermore, there are four simulations with alternating FW forcing in a single ocean basin: *AMOC*$\pm^c$, *SOMOC*$\pm^c$, *AMOC*$\pm^m$, and *SOMOC*$\pm^m$. Finally, two model runs use the alternating FW forcings applied simultaneously to the North Atlantic and the Southern Ocean sinking regions: *MIXVAR1* and *MIXVAR2* (Table 2).

The mean state of the meridional overturning stream functions in the Pacific and the Atlantic prior to the FW forcing is shown in Figures 4a and 4b. Figures 4c–4m show the FW forcing and anomalies in the individual meridional overturning circulation cells of the North Atlantic, the Southern Ocean, and the North Pacific, respectively. The perturbations in the overturning circulation cells generate substantial changes in meridional heat transport and are thus associated with large-scale climate change. Here we will focus solely on the effects of ocean circulation changes on the seawater ϵ_{Nd} distribution. Details regarding overturning-induced

©2014. American Geophysical Union. All Rights Reserved.

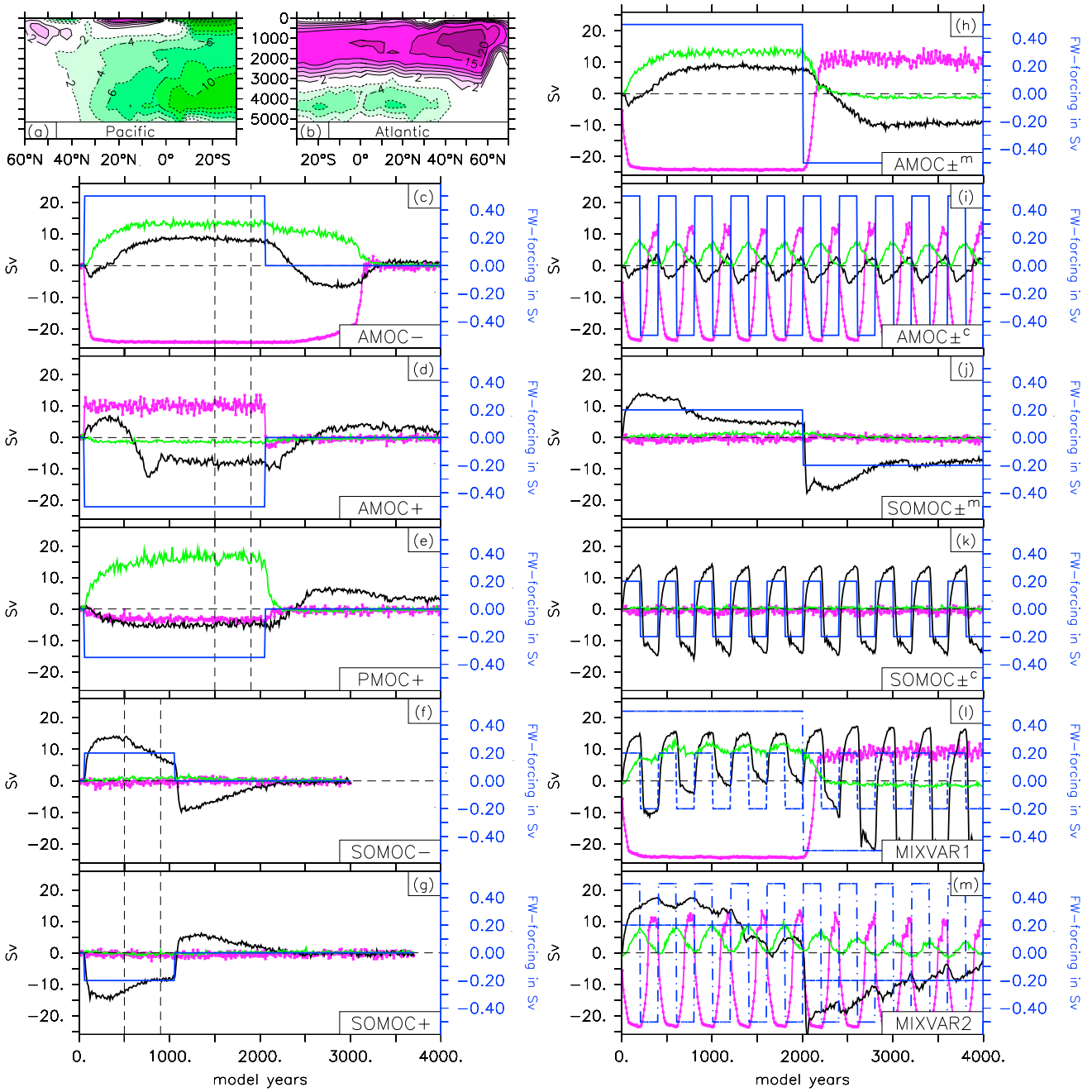

Figure 4. (a and b) Mean meridional overturning stream function in Sv prior to FW forcing. (c–m) AMOC (pink), SOMOC (black), and PMOC (green) anomalies and FW forcing (blue, right-hand axis) in Sv for model runs indicated in the panels. In Figures 4l and 4m, dashed blue lines indicate FW forcing applied in the Southern Ocean; dash-dotted blue lines depict FW forcing applied in the North Atlantic. See also Table 2 and section 5 for details. Dashed vertical lines in Figures 4a–4e indicate averaging intervals for anomalies shown in Figure 5. All anomalies are calculated with respect to mean state prior to FW forcing.

changes in global climate can be found in e.g., *Menviel et al.* [2008, 2010, 2012], *Bozbiyik et al.* [2011], and *Chikamoto et al.* [2012].

The following paragraph provides details for all model experiments (see also Table 2):

1. Experiment AMOC− is a simulation mimicking ocean circulation changes during Heinrich event 1 [*Hemming*, 2004]. A constant FW hosing of 0.5 Sv was applied for 2000 years (model years 51–2050) over the North Atlantic (see Figure 1; approximately: 50°N–70°N; 70°W–10°E). The AMOC is strongly reduced to values of about 4 Sv (The strength of the AMOC is defined as the maximum of the meridional

©2014. American Geophysical Union. All Rights Reserved.

stream function in the North Atlantic.) (Figure 4c). This weak state lasts for about 3000 years in qualitative agreement with Pa/Th data from the North Atlantic by *McManus et al.* [2004].

2. The idealized forcing in experiment AMOC+ is opposed to the one in AMOC−. FW is extracted at a constant rate of 0.5 Sv from the North Atlantic for 2000 years. The associated buoyancy anomalies result in an AMOC strengthening of about 10 Sv (Figure 4d).
3. Experiment PMOC+ (Figure 4e) shows the contribution of deep water formation in the North Pacific to ϵ_{Nd} changes in the Pacific. FW is extracted at a constant rate of 0.35 Sv from the region: 45°N–65°N; 145°E–135°W for 2000 model years. The resulting PMOC anomalies reach ∼16 Sv.
4. A weakening of the Southern Ocean Meridional Overturning (SOMOC), for example, in response to an Antarctic ice sheet instability [*Menviel et al.*, 2010; *Weber et al.*, 2014] is simulated in experiment SOMOC− (Figure 4f). A highly idealized constant FW hosing of 0.2 Sv is applied for 1000 model years mainly over the Ross and Weddell Sea (namely: 62°S–80°S; 160°E–10°E).
5. A strengthening of the SOMOC is generated in experiment SOMOC+ (Figure 4g). The FW forcing is opposite to the one in experiment SOMOC−. This run partly simulates conditions as hypothesized for the glacial ocean with a stronger influence of bottom water of southern origin [*Lynch-Stieglitz et al.*, 2007; *Lund et al.*, 2011].

Four runs with alternating FW forcing are conducted in order to study the local correlation and lead-lag relationships between the AMOC/SOMOC and ϵ_{Nd} anomalies on a centennial scale (AMOC$\pm^{c}$, SOMOC$\pm^{c}$) and a millennial scale (AMOC$\pm^{m}$, SOMOC$\pm^{m}$), respectively. Anomalous FW forcing is applied in the North Atlantic (0.5 Sv) and the Southern Ocean (0.2 Sv), respectively, for 200 (centennial scale) and 2000 (millennial scale) model years. Subsequently, FW is extracted at the same rate for the same time. The forcing regions are identical to the ones mentioned above. The response of the MOC in the different ocean basins is shown by Figures 4h–4k. Global maps of correlations between the alternating MOC indices and the local ϵ_{Nd} anomalies are calculated at lags ranging from 0 to 1000 model years (0 to 200 model years for centennial scale) to determine the relationship between ocean circulation changes and ϵ_{Nd} anomalies in various regions.

Finally, two model runs are conducted in which the alternating FW forcings of the four above mentioned simulations are applied simultaneously to the North Atlantic or the Southern Ocean sinking regions (Figures 4l and 4m). The run MIXVAR1 combines the centennial-scale FW forcing of the SOMOC (as in SOMOC$\pm^{c}$) and the millennial-scale forcing of the AMOC (as in AMOC$\pm^{m}$) and vice versa in MIXVAR2. Note, however, that the circulation anomalies are far from being a simple superposition of the simulations with separate alternating forcing. In particular, the amplitude of centennial-scale SOMOC variability is strongly enhanced when the AMOC is in a stronger-than-normal phase (Figure 4l). The reasoning behind this approach is that AMOC and SOMOC changes may have occurred at the same time in the past which could significantly complicate their respective detection using ϵ_{Nd}. Thus, these simulations will help determine the covariability between ocean overturning changes and ϵ_{Nd} anomalies when changes in Northern and Southern source waters occur simultaneously.

It needs to be emphasized that in all experiments a fraction of the FW forcing that is applied over one region can be advected to other regions of the world ocean. For example, anomalous FW forcing applied in the North Atlantic in experiment AMOC+ can be advected to the Southern Ocean. This can cause anomalies in the Antarctic bottom water (AABW) formation (Figure 4c). Even though this represents a potentially realistic scenario in the context of past ocean circulation changes, it makes it challenging to completely disentangle the individual contribution of the respective overturning anomalies in terms of ϵ_{Nd} changes.

6. Results and Discussion

6.1. ϵ_{Nd} Fingerprints of MOC Changes

The simulated overturning changes induced by FW forcing result in substantial ϵ_{Nd} anomalies in various ocean regions. Figure 5 depicts zonal means of simulated ϵ_{Nd} anomalies and the corresponding simulated overturning cells for the Atlantic and the Pacific, respectively. The temporal averaging intervals for the zonal means and the overturning cells are indicated by the dashed vertical lines in Figures 4c–4g. Figure 6 shows the spatially averaged temporal evolution of the ϵ_{Nd} anomalies for five different ocean basins.

In case of an AMOC weakening (*experimentAMOC*−) the supply of North Atlantic waters with very negative values in ϵ_{Nd} to the deep oceans is strongly reduced, thus resulting in positive ϵ_{Nd} anomalies below 1000 m (Figures 5a and 5b). In the Atlantic positive anomalies are largest along the path of NADW (2000–3000 m,

©2014. American Geophysical Union. All Rights Reserved.

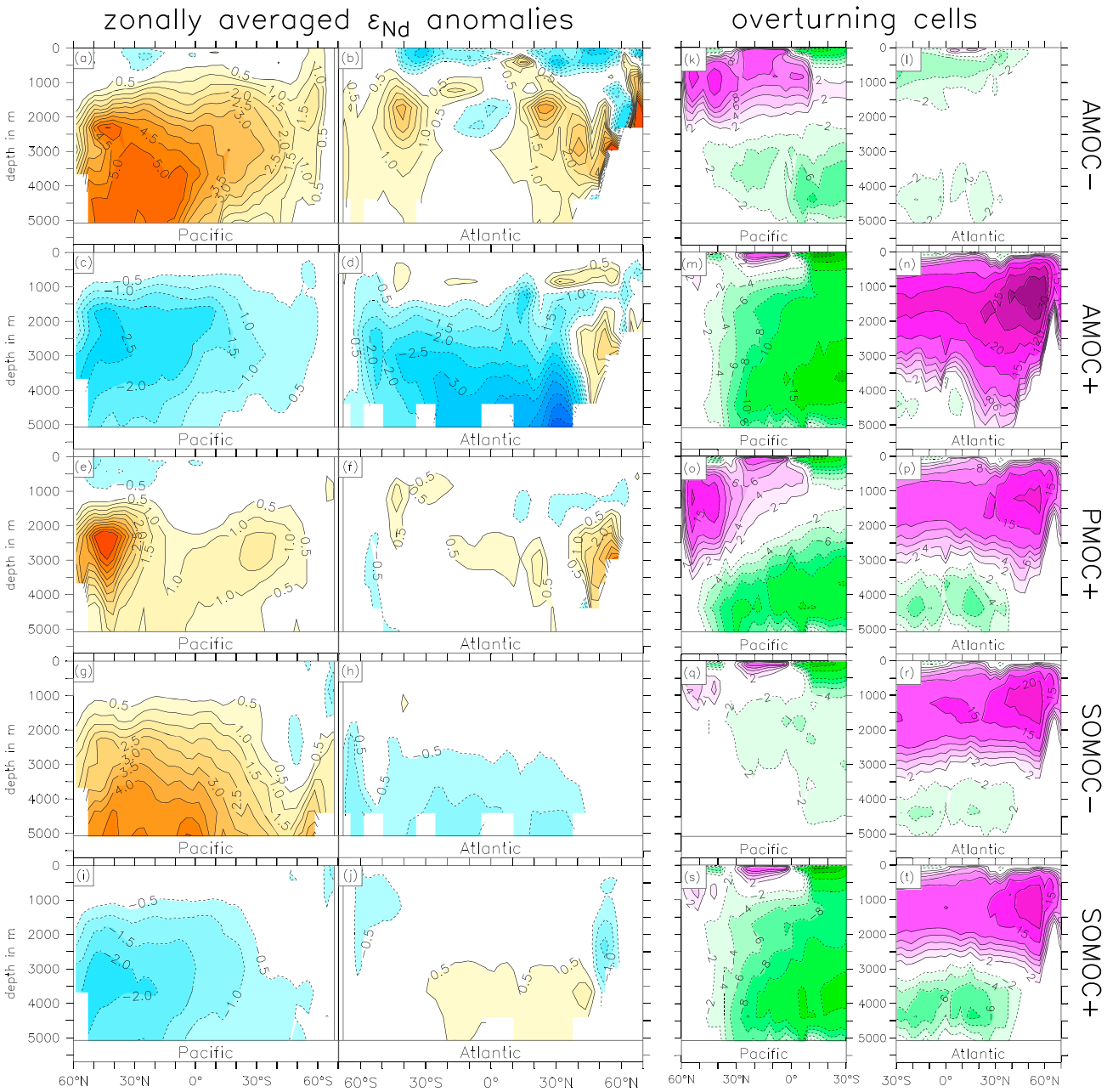

Figure 5. (a–j) ϵ_{Nd} anomalies averaged over Pacific (Figures 5a, 5c, 5e, 5g, 5i) and Atlantic (Figures 5b, 5d, 5f, 5h, 5j) for model experiments as indicated on the right-hand side with respect to mean state prior to FW forcing. (k–t) Strength of meridional overturning stream function (Sv) for Pacific (Figures 5k, 5m, 5o, 5q, 5s) and Atlantic (Figures 5l, 5n, 5p, 5r, 5t) for model experiments as indicated on the right-hand side. See dashed vertical lines in Figures 4c–4g for temporal averaging intervals. The mean meridional overturning stream functions for the Pacific and the Atlantic prior to the FW forcing are shown in Figures 4a and 4b.

not shown). The largest positive ϵ_{Nd} anomalies are found in the deep North Pacific attaining values of up to 5 units (Figure 5a). The temporal evolution of simulated ϵ_{Nd} anomalies exhibits that anomalies in the deep North Pacific develop with a delay of several hundred years compared to the ones in the North Atlantic (Figures 6f and 6k). In the Northern Indian Ocean anomalies reach 0.5–1.0 units (Figure 6z). Simulated positive anomalies of about 1 unit in the deep South Atlantic are in good agreement with *Piotrowski et al.* [2008] (their Figure 3) who found a similar increase for H1, H4, and H6 for high-resolution records of the sediment cores RC11-83 (41.60°S, 9.72°E, 4718 m) and TNO57-21 (40.13°S, 7.82°E, 4981 m), respectively (Figure 2q). Anomalies of similar magnitude were found in the intermediate South Atlantic for H1 by

©2014. American Geophysical Union. All Rights Reserved.

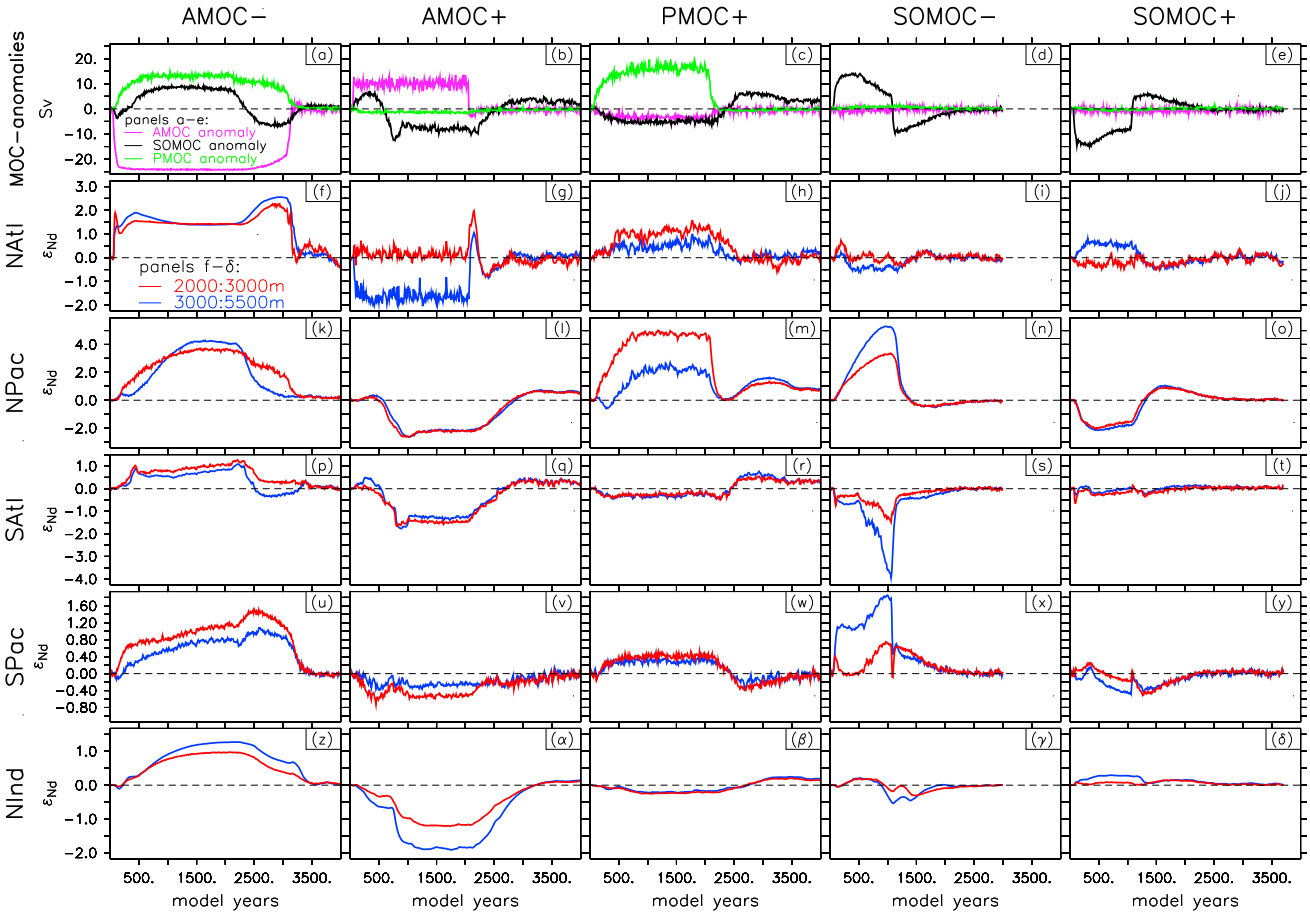

Figure 6. (a–e) MOC anomalies in Sv and (f–δ) ϵ_{Nd} anomalies averaged over different ocean basins and depths of 2000–3000 m (red) and 3000-5500 m (blue) for model experiments indicated above the panels. The ocean basins are NAtl (Figures 6f–6j): 60°W–15°E, 30°N–70°N; NPac (Figures 6k–6o): 130°E–120°W, 45°N–65°N; SAtl (Figures 6p–6t): 60°W–15°E, 45°S–70°S; SPac (Figures 6u–6y): 150°E–70°W, 45°S–70°S; and NInd (Figures 6z–6δ): 45°E–100°W, 0°N–30°N. Anomalies are calculated with respect to mean state prior to FW forcing.

Pahnke et al. [2008] (core: KNR159-5-36GGC; 27.51°S, 46.47°W, 1268 m, Figure 2g) which is reproduced by our AMOC− experiment.

Near the surface of the North Atlantic negative anomalies prevail as less water low in ϵ_{Nd} is exported to the deep ocean compared to the strong AMOC case. In the subtropical North Atlantic the simulation exhibits positive anomalies below 1000 m and negative anomalies at shallower depths (Figure 5b). With regard to shallow water depths, however, it should be kept in mind that our simplified modeling approach cannot account for additional ϵ_{Nd} anomalies that may be caused by changes in dust input or river runoff during an AMOC weakening. Confidence in our results is provided by the fact that this change of sign of the ϵ_{Nd} anomalies can also be found in paleorecords for H1 and the Younger Dryas. The core MD99-2198 [*Pahnke et al.*, 2008] from 1330 m shows a positive anomaly of about 1 unit during H1 and YD (Figure 2h) whereas the shallower core KNR166-2-26JPC (546 m) [*Xie et al.*, 2012] exhibits negative ϵ_{Nd} anomalies for these events (Figure 2d). The core KNR166-2-31JPC (751 m) [*Xie et al.*, 2012] exhibits a negative anomaly for the YD and an alternating behavior during H1 (Figure 2e).

The ϵ_{Nd} anomalies in the deep Pacific in experiment AMOC− can only partly be regarded as a direct consequence of the NADW weakening. In our simulation, the AMOC weakening and the associated reorganizations in the atmosphere result in a substantial strengthening of the meridional overturning in the North Pacific (Figure 5k and green line in Figure 4c) which is qualitatively in good agreement with reconstructions for Heinrich event 1 [*Okazaki et al.*, 2010]. Details on the teleconnections that lead to a PMOC strengthening can be found in *Chikamoto et al.* [2012]. With regard to changes in the deep Pacific ϵ_{Nd}

©2014. American Geophysical Union. All Rights Reserved.

values, an intensified PMOC works in the same direction as a NADW weakening as the transport of water high in ϵ_{Nd} to water depths of 1000–2000 m in the North and South Pacific is substantially increased. In order to elucidate the contribution of a stronger PMOC to the ϵ_{Nd} anomalies, an intensification of deep water formation in the North Pacific was generated by FW extraction in this region (experiment: PMOC+, Figures 4e and 5o). The overturning anomalies in the PMOC+ run are about 3 Sv stronger compared to the ones generated by the simulated AMOC cessation. They cause a substantial increase in ϵ_{Nd} values in the Pacific below 2000 m (Figure 5e). Figures 6k and 6m show that the magnitude and temporal evolution of the deep North Pacific ϵ_{Nd} anomalies in AMOC− can mainly be attributed to the PMOC strengthening. In the South Pacific, however, the increase in the PMOC cannot explain the magnitude of the anomalies (Figures 6u and 6w). In this region the positive anomalies are mainly driven by the decreased supply of the negative NADW end-member. Furthermore, a fraction of the FW forcing of the AMOC− simulation is advected from the North Atlantic to the Southern Ocean and leads to a SOMOC weakening that results in positive ϵ_{Nd} anomalies. Details on the effect of SOMOC anomalies will be given below.

Small positive ϵ_{Nd} anomalies in the deep North Atlantic (Figure 5f) are generated by the fact that in response to the PMOC strengthening the surface branch of the global conveyor belt weakens [*Menviel et al.*, 2012] which results in a reduction of NADW formation (Figure 4e).

The AMOC+ experiment is characterized by negative ϵ_{Nd} anomalies in almost the entire water column (Figures 5c and 5d) as a strengthening in the NADW production (Figure 5n) increases the contribution of the negative end-member to the global water mass distribution. In the Atlantic, the largest negative anomalies of ∼4 ϵ units are found at depths that are normally occupied by AABW. Figures 6b and 6g show that even the increased decadal variability, which the stronger-than-normal AMOC causes, can be identified in the deep North Atlantic ϵ_{Nd} anomalies. In the Pacific and the Indian Ocean (Figures 5c and 6l α) ϵ_{Nd} anomalies reach −2 units. Here the temporal evolution of the anomalies is also influenced by the overturning in the Southern ocean that exhibits an alternating behavior over the first 1000 model years in response to the FW forcing in the North Atlantic (Figure 4d). The simulated ϵ_{Nd} anomalies that occur in response to an AMOC weakening and strengthening, respectively, are qualitatively in very good agreement with the one presented by *Rempfer et al.* [2012a] for their experiment NA2k030Sv that use alternating FW forcing in the North Atlantic with an amplitude of 0.3 Sv and a period of 2000 years (their Figure 8).

Changes in the strength of the Southern Ocean meridional overturning (*experiments SOMOC− and SOMOC+*) result in a seesaw pattern of simulated ϵ_{Nd} anomalies in the deep Pacific and the deep Atlantic, respectively (Figures 5g–5j). Modern AABW is characterized by intermediate values of ϵ_{Nd} (−7 to −11) [*Lacan et al.*, 2012; *Stichel et al.*, 2012; *Carter et al.*, 2012]. Thus, a decrease (increase) in AABW formation leads to a strengthened (weakened) influence of the two end-members of ϵ_{Nd} in the respective ocean basin. In particular, the North Pacific is subject to substantial ϵ_{Nd} anomalies. These results confirm the findings of *Rempfer et al.* [2012a] that reported a similar Atlantic Pacific dipole response in ϵ_{Nd} for millennial-scale SOMOC changes (their experiment SO2k030Sv and their Figure 11). Our simulation shows that a weakened AABW formation causes a strong imprint on ϵ_{Nd} values in the South Atlantic at depths below 2000 m (Figure 6s). This challenges previous interpretations of data from the Cape Basin [*Rutberg et al.*, 2000; *Piotrowski et al.*, 2004, 2008] that assumed temporal variations in ϵ_{Nd} to primarily reflect changes in NADW. For example, the Antarctic Cold Reversal [*Barker et al.*, 2009] around ∼14.5–13 k.a. B.P. may have been caused by a weakening of the SOMOC generated by an instability of the Antarctic ice sheet [*Weaver et al.*, 2003; *Menviel et al.*, 2011]. Thus, it remains uncertain to what extent negative anomalies recorded in the core RC11-83 [*Piotrowski et al.*, 2004] (Figure 2q) around this time indicate an NADW strengthening or AABW weakening or a superposition of both. Our results—in line with the results of *Rempfer et al.* [2012a]—suggest a weakened SOMOC and a strengthened AMOC, respectively, to generate anomalies of opposite sign in the deep North Pacific (Figures 5c and 5g). Additional ϵ_{Nd} records from this region would help elucidate the potential individual contributions of the two overturning cells.

6.2. Quantitative Reconstructions of MOC Changes Through ϵ_{Nd} Data

Thus far our results have helped to identify the transient basin-average response of ϵ_{Nd} to several ocean circulation changes induced by FW forcing. Here we raise the question whether the temporal behavior of the individual MOCs can be determined from compilations of paleo ϵ_{Nd} records from different regions. Figure 6, for example, indicates that the shape of ϵ_{Nd} time series does not necessarily resemble the temporal evolution of the MOC indices. In fact, in the modeling study by *Rempfer et al.* [2012a] it was concluded that it is

©2014. American Geophysical Union. All Rights Reserved.

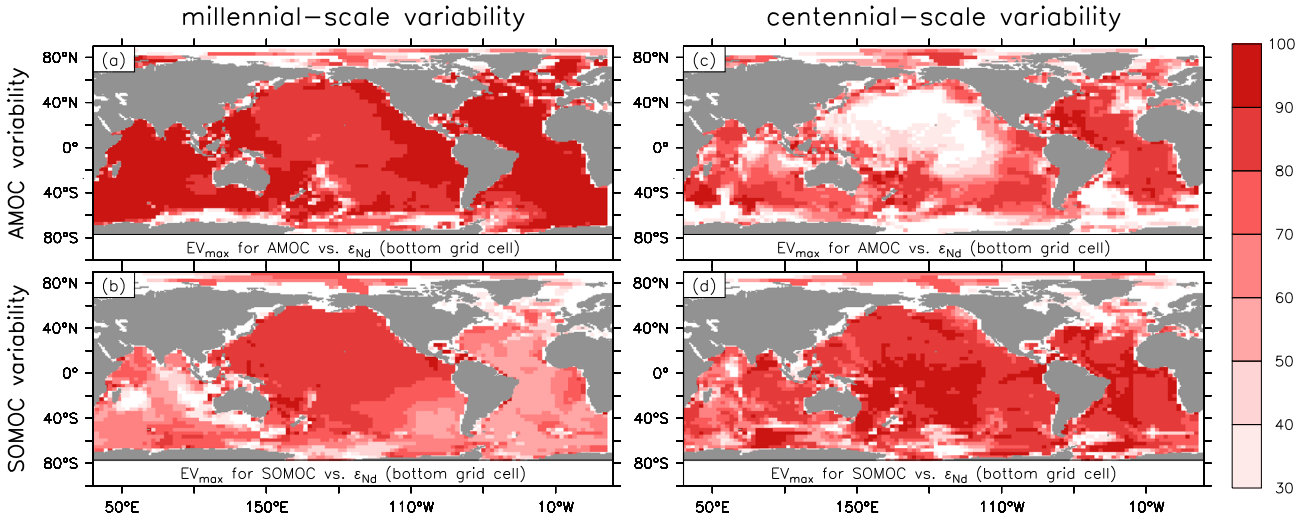

Figure 7. (a) Maximum of bottom cell explained variance (EV_{max}) in % derived from lagged local correlation between AMOC index and simulated ϵ_{Nd} for experiment AMOC$\pm^{m}$. (b) Bottom cell EV_{max} in % derived from lagged local correlation between SOMOC index and simulated ϵ_{Nd} for experiment SOMOC$\pm^{m}$. (c, d) Same as Figures 7a and 7b, respectively, for centennial-scale MOC variability (experiments: AMOC$\pm^{c}$ and SOMOC$\pm^{c}$). Indices of Meridional Overturning Circulation lead in lagged correlation.

difficult to derive the AMOC strength from ϵ_{Nd}, whereas a more pronounced relationship was found to exist for the SOMOC. Our global modeling approach enables us to identify potentially promising future core locations and to elucidate the key spatial fingerprints of AMOC and SOMOC changes. This information can in principle be used to invert ϵ_{Nd} records and to reconstruct past ocean circulation changes quantitatively.

The experiments AMOC$\pm^{c}$, SOMOC$\pm^{c}$, AMOC$\pm^{m}$, and SOMOC$\pm^{m}$ were driven by alternating FW forcing to generate 10 centennial- (AMOC$\pm^{c}$ and SOMOC$\pm^{c}$) and one millennial-scale (AMOC$\pm^{m}$ and SOMOC$\pm^{m}$) weakening-strengthening cycle, respectively, over the course of 4000 model years. Figures 4h–4k shows the time series of the MOC indices. Local correlations between the AMOC and SOMOC indices, respectively, and the ϵ_{Nd} changes in the global model domain are then computed for the seafloor grid cells taking into account potential lags of 0 to 200 (1000) years between the centennial (millennial)-scale MOC changes and the simulated-ϵ_{Nd} anomalies. In case of an alternating overturning in the North Atlantic, the maximum of the explained variance (EV, square of the local correlation) at the seafloor occurs in the Atlantic and the Indian Oceans (Figures 7a and 7c). Here the EV reaches values of 70–100% and is larger for the millennial-scale variability. The maximum of the EV in the Atlantic occurs at minimum lags of less than 300 years in the AMOC$\pm^{m}$ run (not shown). The shortest lags occur around grid cells in the vicinity of the NADW Deep Western Boundary Current (DWBC). The lags at which the ϵ_{Nd} responds to MOC changes are shorter than the advective timescales for the respective locations. Due to the proximity of the DWBC to the influence of the continental ϵ_{Nd} signature, the seawater ϵ_{Nd} in the DWBC is given by a balance of the continental exchange and the advective strength of the DWBC. Thus, it should be emphasized that the simulated lags in our experiments also depend on the timescale of the highly uncertain BE processes. An AMOC weakening is quickly communicated to other ocean basins via boundary waves, equatorial Kelvin waves, and westward propagating Rossby waves [*Kawase*, 1987; *Johnson and Marshall*, 2002] and via atmospheric teleconnections [*Pahnke et al.*, 2007; *Xie et al.*, 2008] leading to a fast adjustment of the strength of the DWBC ($\delta\vec{u}$) and to a change in the local ϵ_{Nd} advection-exchange balance: $\delta\vec{u}\cdot\vec{\nabla}\overline{\epsilon_{Nd}}$, where $\overline{\epsilon_{Nd}}$ is the local long-term mean value of ϵ_{Nd} in the DWBC. The effect of this advection-exchange balance on the timing of the development of ϵ_{Nd} anomalies can be identified beyond the DWBC. In case of our AMOC− run, ϵ_{Nd} anomalies occur in all ocean basins with maximum lags of a few hundred years (Figures 6a, 6f, 6k, 6p, 6u, and 6z) which is short compared to timescale of the AMOC anomaly of 3000 years even though the simulated deep Atlantic circulation is extremely sluggish for this time. It must be noted that this behavior makes ϵ_{Nd} fundamentally different from another relevant paleoproxy: benthic $\delta^{18}O$. For the latter, the glacioeustatic component was mainly injected into the North Atlantic, and its propagation time to the other ocean basins depends on the state of the AMOC. A recent modeling study [*Friedrich and Timmermann*, 2012] reported a substantial delay

©2014. American Geophysical Union. All Rights Reserved.

in the propagation of the glacioeustatic signal from the North Atlantic source region to the deep ocean in response to an AMOC weakening. The timescale of the delayed propagation that depends mainly on the duration of the AMOC shutdown can thus reach several thousand years potentially compromising the applicability of benthic $\delta^{18}O$ as a global chronostratigraphic correlation tool during times of large-scale ocean circulation changes. In principle, combined, synchronous records of ϵ_{Nd} and benthic $\delta^{18}O$ would be helpful to document the state of the overturning and lead-lag relationships during terminations.

The spatial patterns of the maximum EV at the seafloor differ substantially between the centennial-scale and the millennial-scale AMOC variability in the Pacific. Here seafloor ϵ_{Nd} anomalies explain a large fraction of the AMOC variability in case of millennial-scale changes, whereas the EV turns out to be marginal in the AMOC$\pm^c$ simulation (Figures 7a and 7c). As explained above, in case of an AMOC weakening the ϵ_{Nd} increase in the deep Pacific is largely driven by the development of a PMOC which lags the AMOC weakening by several hundred years (Figure 4h). In case of an AMOC strengthening ϵ_{Nd} values in the deep North Pacific decrease with a delay of several hundred years (Figure 6l). In the millennial-scale experiment, both delays in the ϵ_{Nd} response in the deep North Pacific are relatively short compared to the overall timescale of the AMOC weakening-strengthening cycle. In case of the centennial-scale variability, however, the duration of the AMOC strengthening phase in the AMOC$\pm^c$ run turns out to be too short to cause a decrease in deep North Pacific ϵ_{Nd} values. Thus, ϵ_{Nd} anomalies are mainly determined by the PMOC response during the AMOC weakening phase. Figure 4i, however, exhibits that one PMOC strengthening cycle has the same timescale as one AMOC weakening-strengthening cycle which leads to out-of-phase ϵ_{Nd} anomalies during the strong AMOC phase.

The deep Pacific appears to be the most promising region for reconstructing the temporal evolution of overturning changes in the Southern Ocean from ϵ_{Nd}. Here seafloor ϵ_{Nd} changes can explain 70–90% of SOMOC anomalies (Figures 7b and 7d). Local correlations in the deep Southern Ocean are substantially lower. The reason for this counterintuitive behavior can mainly be found in the fact that the deep Southern Ocean appears to be "saturated" with AABW regardless of the SOMOC strength. Thus, an increase in the SOMOC is not reflected in deep Southern Ocean ϵ_{Nd} values (see also Figures 5i, 5j, 6t, and 6y). However, this behavior may partly be caused by the simplified ϵ_{Nd} approach employed here.

Another interesting feature can be seen in the deep Atlantic. Figures 7b and 7d shows that EV is substantially higher for the centennial-scale SOMOC variability compared to millennial-scale changes. This difference can be explained in terms of the different responses of the SOMOC to FW forcing on the longer and shorter timescales. Figure 4j shows that the amplitude of the millennial-scale SOMOC weakening is reduced by about 50% after ~500 years although the FW forcing remains unchanged. A similar behavior can be observed for the SOMOC strengthening. This indicates that internal reorganizations of the deep ocean currents are at work that lead to a more complex response in the millennial-scale case compared to the centennial-scale variability where the SOMOC closely follows the FW forcing.

In addition to the general overview given above, we specifically tested the locations of the cores that currently provide ϵ_{Nd} data for Termination I (Table S1 and Figure 2) with respect to their potential to reconstruct AMOC and SOMOC changes. Table S1 shows the maximum correlations between the simulated MOC index and the simulated ϵ_{Nd} anomalies at this model grid point and the lag at which this maximum correlation is reached. The cores in the North Atlantic exhibit mainly very high correlations for an AMOC variability in particular if this variability occurs on a millennial timescale. Here values are well above 0.8 irrespective of the core location and depth. The lag at which this correlation is reached is small compared to the overall timescale of the AMOC weakening-strengthening cycle. The North Pacific core seems to be well located to capture AMOC changes. However, the restriction must be mentioned that, due to its shallow location, the core may also be subject to ϵ_{Nd} anomalies caused by changes in dust deposition and river runoff that are not taken into account in our simulation.

The core in the deep Indian Ocean exhibits the largest lag of 550 years, respectively, for detecting millennial-scale AMOC changes and a very high correlation of −0.97.

The correlations reported in Table S1 for the model simulations with alternating FW forcing appear to be promising for several core locations. For a reconstruction of past MOC changes, however, using more than one core location will give a more robust result. Furthermore, according to our findings and the results of *Rempfer et al.* [2012a] taking into account ϵ_{Nd} anomalies in the North Atlantic and North Pacific can help

©2014. American Geophysical Union. All Rights Reserved.

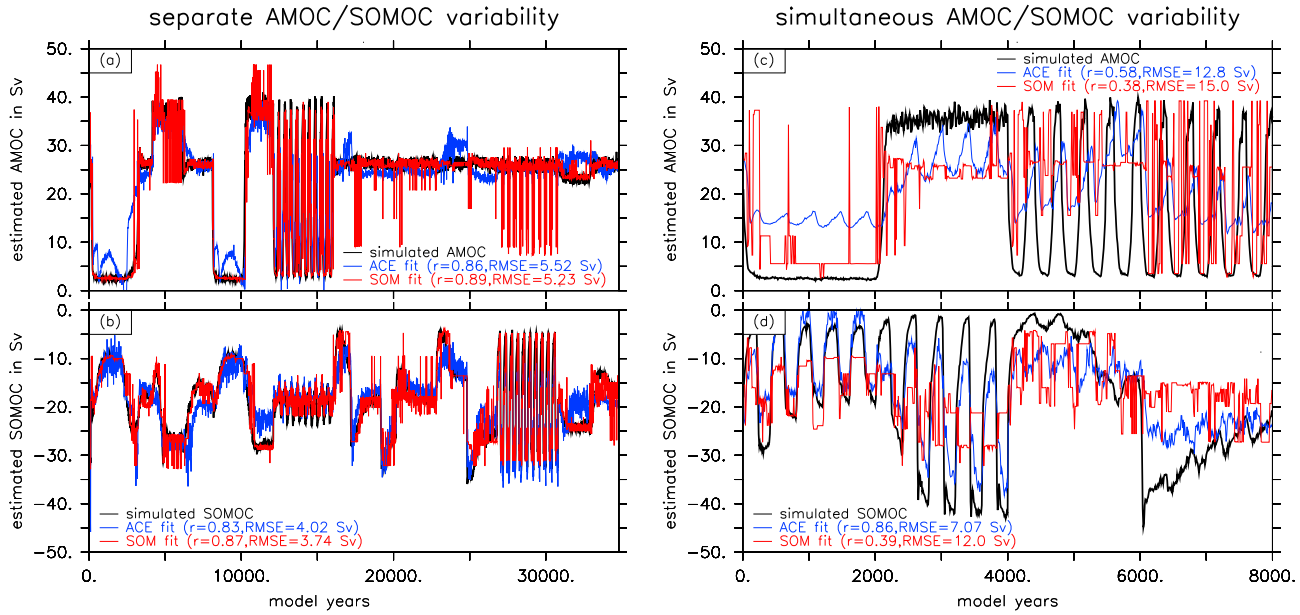

Figure 8. (a and b) Data used for fit and validation were taken from model runs of separate FW forcing of North Atlantic or Southern Ocean sinking regions. (c and d) Validation against data of model runs of simultaneous FW forcing of North Atlantic or Southern Ocean sinking regions (Figures 4l and 4m). Overturning cell and fitting techniques as indicated in the panels. See text, Table 2, and Figure 4 for details on the model simulations. Please see text for details and references regarding the fitting techniques.

distinguish between AMOC and SOMOC changes. Thus, a methodology that combines different ϵ_{Nd} core records would be desirable. For this procedure, we use two different nonparametric regression methods: the Alternating Conditional Expectation Value (ACE) algorithm [*Breiman and Friedman*, 1985; *Timmermann et al.*, 2001] and a Self-Organizing Map (SOM) [*Kohonen*, 1982; *Friedrich and Oschlies*, 2009a, 2009b]. Details on the regression methods are provided in the supporting information.

The simulated MOC data and the simulated ϵ_{Nd} at the core locations from the following simulations: AMOC+, AMOC−, PMOC+, SOMOC+, SOMOC−, AMOC$\pm^c$, SOMOC$\pm^c$, AMOC$\pm^m$, and SOMOC$\pm^m$ were concatenated providing a total of 34,800 model years. The core locations used for the accuracy assessment of the MOC reconstruction were preselected according to their explained variance (Table S1), and cores from water depths above 800 m were excluded as near surface processes such as dust input and river runoff are not taken into account in our ϵ_{Nd} parametrization. Subsequently, different combinations of simulated ϵ_{Nd} data at the sediment core locations (Figure 1) were tested with regard to the accuracy of the ACE- and SOM-derived MOC reconstructions. Here we ensured that data from at least two different ocean basins were included. Finally, a combination of three core locations for AMOC and SOMOC reconstructions, respectively, was identified. For the empirically derived AMOC, simulated ϵ_{Nd} data were used that correspond to the core locations of ODP-980 (55.4833°N/14.7000°W), RC11-83 (41.0700°S/9.7170°E), and BOW-8A (54.7833°N/176.9167°E). The modeled SOMOC was reconstructed using simulated ϵ_{Nd} data from the core locations KNR159-5 (27.8500°S/46.7833°W), BOW-8A (54.7833°N/176.9167°E), and SK129-CR2 (3.0000°N/76.0000°E). More details on the core locations are provided in Figure 1 and Table 1.

Figures 8a and 8b show the quality of the simulated reconstructions when simultaneously occurring changes in the AMOC and SOMOC are not explicitly taken into account. As anticipated from the correlations presented in Table S1 skillful empirical MOC reconstructions can be achieved with both techniques. For the simulated AMOC the correlation amounts to 0.86 (ACE) and 0.89 (SOM), respectively. The simulated SOMOC can be empirically reconstructed with correlations of 0.83 (ACE) and 0.87 (SOM). The skill of the reconstructions heavily deteriorates when changes in the other overturning cells occur at the same time. Applying the above mentioned fit to ϵ_{Nd} data of the model runs MIXVAR1 and MIXVAR2 results in substantially larger RMS errors and substantially smaller correlations (Figures 8c and 8d).

©2014. American Geophysical Union. All Rights Reserved.

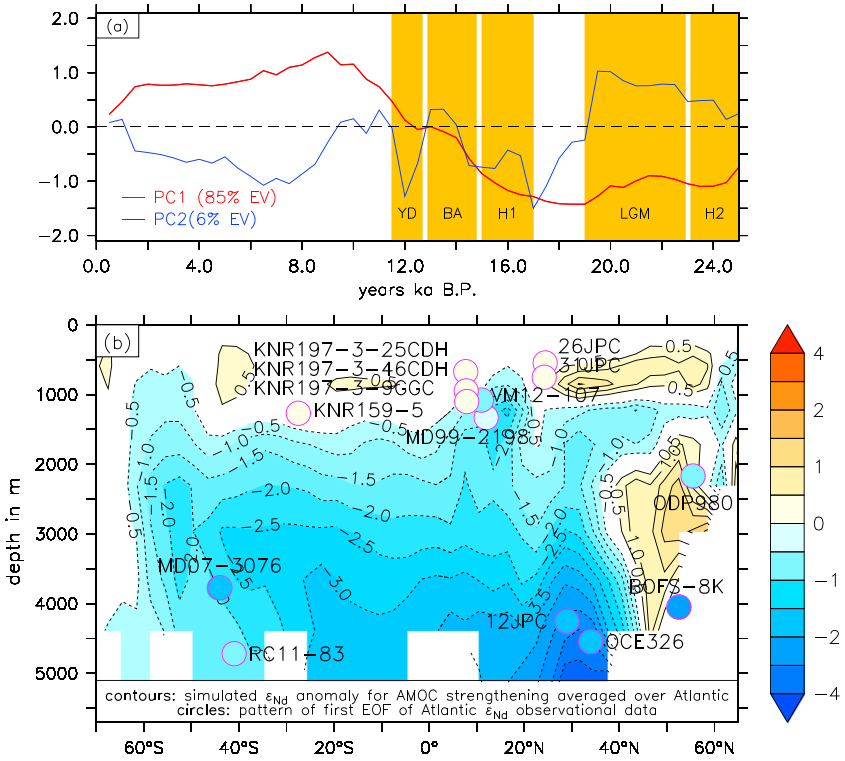

Figure 9. (a) Principal components of the first (red) and second (blue) EOF of Atlantic paleo ϵ_{Nd} records (Table 1) for the Last Glacial Termination. The first (second) EOF explains 85% (5%) of the variance. (b) Pattern of the first EOF (circles) and zonally averaged Atlantic ϵ_{Nd} anomalies (shaded) for an AMOC strengthening (experiment AMOC+, identical to Figure 5d). The colorbar refers to the EOF pattern. Values for ϵ_{Nd} anomalies are given by the contour labels.

6.3. Implications for Termination I

Attempts have been made to reconstruct the overall chronology of millennial-scale changes in the North Atlantic [*McManus et al.*, 2004], the North Pacific [*Okazaki et al.*, 2010], and Southern Ocean [*Menviel et al.*, 2011] overturning cells during the Last Glacial Termination. The well-known sequence of Heinrich Event 1, Bølling Allerød/Antarctic Cold Reversal and the Younger Dryas can be distinguished in most ϵ_{Nd} records from depths between 500 and 2200 m, and the sign of the recorded anomalies can be reproduced by our simulated large-scale anomaly patterns. Numerous studies have reported a decrease in ϵ_{Nd} in various ocean basins between the Last Glacial Maximum and the Holocene [*Rutberg et al.*, 2000; *Piotrowski et al.*, 2004; *Gutjahr et al.*, 2008; *Piotrowski et al.*, 2009; *Roberts et al.*, 2010; *Horikawa et al.*, 2010; *Piotrowski et al.*, 2012] (Figure 2).

Overall, our model results clearly support the notion that this observed change can be attributed to an increasing contribution of NADW to the water mass distribution of the deep ocean.

Figure 9 shows an empirical orthogonal function (EOF) of the Atlantic paleo ϵ_{Nd} records for Termination I and compares the spatial pattern of the first EOF with the ϵ_{Nd} anomalies simulated for an AMOC strengthening (experiment AMOC+, same as in Figure 5d). The first EOF explains 85% of the total variance and exhibits a transition toward more negative ϵ_{Nd} in the deep ocean over the course of Termination I. The beginning of this transition coincides with the end of H1 (Figure 9a) in agreement with radiocarbon records of *Barker et al.* [2010] that suggest a deepening of the AMOC around this time. The spatial pattern of the first EOF (Figure 9b) is well reflected by the simulated ϵ_{Nd} anomaly pattern generated by an AMOC strengthening. The increased contribution of the negative North Atlantic end-member leads to large negative ϵ_{Nd} anomalies in the deep Atlantic and to weak positive anomalies in some regions of the upper water column of the Atlantic.

The discrepancy around core ODP-980 can be partly explained by the zonal average shown in the figure. The sign of the ϵ_{Nd} anomalies is consistent with the EOF pattern at the true core location of 14.7°W (not shown).

©2014. American Geophysical Union. All Rights Reserved.

In addition it should be noted that core ODP-980 is located in a strong spatial gradient of continental values of ϵ_{Nd} (Figure 1) which may lead to an intricate response to AMOC changes that cannot be fully represented by the coarse-resolution Earth system model. The bottom topography around core BOFS-8K is characterized by large spatial variability. The sea floor drops by about 3000 m over only ~3° of latitude—roughly the resolution of the ocean model—from the Rockall Bank to the core location. Thus, the model simulation cannot capture the recorded response at the core location.

Overall, the amplitude of the ϵ_{Nd} anomaly in the deep Atlantic that occurs in response to an AMOC strengthening in our model simulation accounts for only half of the amplitude recorded in the ϵ_{Nd} cores. (Please note that the spatial EOF1 pattern of the core data in Figure 9b needs to be multiplied with the PC1 in Figure 9a in order to attain the full amplitude.) The next section seeks to explain this mismatch and discusses additional challenges in the interpretation of modeled and recorded ϵ_{Nd} data.

6.4. Caveats, Limitations, and Implications for Interpreting Observed ϵ_{Nd} Data

Some caveats and inconsistencies on both the observational and modeling sides need to be discussed, in order to interpret and evaluate our results in the context of observational records for the Last Glacial Termination. On the modeling side it is mainly the parametrization of ϵ_{Nd}, the representation of global teleconnections, and the overall model performance that contribute substantially to the robustness of the simulated ϵ_{Nd} response to overturning changes and thus to its evaluation as a water mass tracer.

For example, one apparent discrepancy between the ϵ_{Nd} paleorecords and our simulations is the lack of millennial-scale AMOC variability in most deep ocean cores during the Last Glacial Termination, whereas high-simulated correlations are found for locations of cores deeper than 2500 m (Table S1) for the experiments AMOC$\pm^{c}$ and AMOC$\pm^{m}$. AMOC anomalies are estimated to have been in the order of 12–14 Sv for H1 and the Younger Dryas [*Ritz et al.*, 2013] and are thus comparable to the ones generated in our simulations. One reason may be the lack of temporal resolution in the deep ocean cores. Another potential explanation can be found in the strong AMOC that governs the preindustrial setup of our experiments (Figure 4b). North Atlantic overturning is believed to have been shallower during the LGM compared to the Holocene [*Curry and Oppo*, 2005; *Lynch-Stieglitz et al.*, 2007; *Roberts et al.*, 2010; *Lippold et al.*, 2012] reaching water depths of only ~2000 m. In a situation of a shallower North Atlantic overturning the overall contribution of a water mass produced in the North Atlantic to the deep ocean would be smaller. Thus, a reduction or cessation of a shallower North Atlantic overturning would not result in major changes of the deep ocean water mass distribution and thus deep ocean ϵ_{Nd} values. We speculate that strong AMOC simulated in our preindustrial setup is also responsible for the underestimation of the ϵ_{Nd} anomaly during an AMOC strengthening. The amplitude simulated in response to an AMOC strengthening reaches ~2–3 units in most regions of the deep Atlantic with a maximum of 5.5 units at 30°N below 4000 m (Figure 9b, shaded values). The decrease in ϵ_{Nd} recorded in the cores (Figure 2) that is usually interpreted as a stronger influence of NADW in the deep Atlantic is in the order of ~3–6 units.

The parametrization of ϵ_{Nd} BE in our experiments also adds to the uncertainties in the ϵ_{Nd} response. As pointed out above, the temporal evolution of ϵ_{Nd} in particular in the vicinity of BE grid points is largely determined by the strength of advection, the ϵ_{Nd} value of the advected water, and the strength of the BE. Therefore, both magnitude and timescale of the ϵ_{Nd} response to overturning changes are functions of the BE parametrization. In view of evidence for spatially varying BE [*Wilson et al.*, 2013] and influence of BE at depths of 4000 m [*Wilson et al.*, 2012] which are not taken into account in our simulations, future studies are needed to reassess the robustness of the results.

The representation of global teleconnections in the atmosphere and the ocean (e.g., the response of wind fields and moisture transport to changes in sea surface temperature) has also an impact on the simulated response to overturning changes and hence the one of simulated ϵ_{Nd}. For example, our results reveal strong and deep-reaching positive ϵ_{Nd} anomalies in the North Pacific in response to an AMOC shutdown (Figure 5a). These anomalies are in agreement with the results of *Rempfer et al.* [2012a] and are caused by a strengthening of the PMOC. In case of *Rempfer et al.* [2012a], however, the absence of a dynamical atmospheric model component a PMOC strengthening response requires an arbitrary retuning of the model's FW balance. It must be noted that the timing and magnitude of the PMOC strengthening and its overall geometry are highly uncertain and model dependent [*Chikamoto et al.*, 2012].

©2014. American Geophysical Union. All Rights Reserved.

The search for promising core locations turns out to be more difficult than what can be assessed in the context of our idealized modeling study. Our modeling results indicate that the North Atlantic DWBC is a very promising location to detect AMOC changes through ϵ_{Nd} records. The core 51GGC (32.7840°N/76.2863°W, 1790 m) was taken in the DWBC [*Gutjahr et al.*, 2008]. Unfortunately, potential ϵ_{Nd} changes due to variations in the water mass distributions may have been—according to *Gutjahr et al.* [2008]—compromised by sediment contributions from shallower waters.

An important question that remains is, how much did a potential decrease in AABW formation over the course of Termination I contribute to the observed shift in deep ocean ϵ_{Nd}? In the deep Atlantic, both an AMOC strengthening and a SOMOC weakening result in simulated negative ϵ_{Nd} anomalies (see also Figures 5d and 5h). Additional paleorecords of ϵ_{Nd} from the deep North Pacific may help to better constrain the role of AABW changes during the Last Glacial Termination as our results suggest that SOMOC and AMOC changes, respectively, are generating ϵ_{Nd} anomalies of opposite sign in this region (Figures 5c and 5g). The fact that the modeling study by *Rempfer et al.* [2012a] came to a similar result based on a different model and a different parametrization of the Nd cycle provides further confidence to this conclusion and our simplified modeling approach.

7. Conclusions

The main findings of our model simulations can be summarized as follows:

1. Our modeling results exhibit substantial ϵ_{Nd} anomalies in response to MOC changes.
2. An AMOC weakening results in a reduced supply of the negative NADW end-member and thus in positive ϵ_{Nd} anomalies below 1000 m. The formation of a PMOC that occurs in response to the AMOC weakening contributes substantially to the large positive ϵ_{Nd} anomalies in the deep North Pacific.
3. Changes in the strength of Southern Ocean overturning result in a Pacific-Atlantic dipole pattern of deep ocean ϵ_{Nd} anomalies with a weakening of the SOMOC leading to negative ϵ_{Nd} anomalies in deep Atlantic and positive ϵ_{Nd} anomalies in deep Pacific.
4. Changes in the strength of the AMOC and the SOMOC, respectively, can be reconstructed using empirical methods with high accuracy from ϵ_{Nd} records in our simulations when the overturning anomalies occur separately.
5. In case of overturning anomalies that occur simultaneously in the North Atlantic and the Southern Ocean the skill of the empirical reconstructions is heavily deteriorated.
6. The local ϵ_{Nd} values are mainly determined by an advection-exchange balance which leads to fast development of ϵ_{Nd} anomalies in response to overturning changes even in a state of a relatively sluggish deep ocean circulation. This makes the response characteristics of ϵ_{Nd} fundamentally different from the glacioeustatic $\delta^{18}O$ signal whose propagation after an injection into the North Atlantic heavily depends on the strength of mean advection.
7. The decrease in deep Atlantic ϵ_{Nd} over the course of the Last Glacial Termination is indicative of an increasing AMOC. However, our results also show that a decreasing SOMOC is acting in the same direction. Additional records from the deep North Pacific may help to determine the contribution of potential changes in Southern Ocean overturning.

The results of our idealized freshwater discharge experiments show the large potential of ϵ_{Nd} records to act as a proxy for past ocean circulation changes in large parts of the seafloor. However, the potential of "contamination" of ϵ_{Nd} data by terrigenous input and redistribution of sediments complicates the search for optimal sediment core locations, and simultaneously occurring overturning changes can make the interpretation of ϵ_{Nd} records challenging.

Acknowledgments
The modeling data for this paper are available by email request to the corresponding author. T. Friedrich is supported by NSF grants 1400914 and 1341311. A. Timmermann is supported by the Japan Agency for Marine-Earth Science and Technology (JAMSTEC) through its sponsorship of the International Pacific Research Center. The authors would like to thank the three anonymous reviewers and the Editor, Heiko Paelike, for their constructive comments. This is IPRC number 1080 and SOEST contribution number 9206.

References

Arsouze, T., J.-C. Dutay, F. Lacan, and C. Jeandel (2007), Modeling the neodymium isotopic composition with a global ocean circulation model, *Chemical Geology*, *239*(1–2), 165–177, doi:10.1016/j.chemgeo.2006.12.006.

Arsouze, T., J.-C. Dutay, M. Kageyama, F. Lacan, R. Alkama, O. Marti, and C. Jeandel (2008), A modeling sensitivity study of the influence of the Atlantic meridional overturning circulation on neodymium isotopic composition at the Last Glacial Maximum, *Clim. Past*, *4*(3), 191–203, doi:10.5194/cp-4-191-2008.

Arsouze, T., J.-C. Dutay, F. Lacan, and C. Jeandel (2009), Reconstructing the nd oceanic cycle using a coupled dynamical biogeochemical model, *Biogeosciences*, *6*(12), 2829–2846, doi:10.5194/bg-6-2829-2009.

Arsouze, T., A. M. Treguier, S. Peronne, J.-C. Dutay, F. Lacan, and C. Jeandel (2010), Modeling the Nd isotopic composition in the North Atlantic basin using an eddy-permitting model, *Ocean Sci.*, *6*(3), 789–797, doi:10.5194/os-6-789-2010.

©2014. American Geophysical Union. All Rights Reserved.

Barker, S., P. Diz, M. J. Vautravers, J. Pike, G. Knorr, I. R. Hall, and W. S. Broecker (2009), Interhemispheric Atlantic seesaw response during the last deglaciation, *Nature*, *457*, 1097–1103.

Barker, S., G. Knorr, M. J. Vautravers, P. Diz, and L. C. Skinner (2010), Extreme deepening of the Atlantic meridional overturning circulation during deglaciation, *Nat. Geosci.*, *3*, 567–571.

Basak, C., E. E. Martin, K. Horikawa, and T. M. Marchitto (2010), Southern Ocean source of ^{14}C-depleted carbon in the North Pacific during the last deglaciation, *Nat. Geosci.*, *3*, 770–773, doi:10.1038/ngeo987.

Bertram, C., and H. Elderfield (1993), The geochemical balance of the rare earth elements and neodymium isotopes in the oceans, *Geochim. Cosmochim. Acta*, *57*(9), 1957–1986, doi:10.1016/0016-7037(93)90087-D.

Bozbiyik, A., M. Steinacher, F. Joos, T. F. Stocker, and L. Menviel (2011), Fingerprints of changes in the terrestrial carbon cycle in response to large reorganizations in ocean circulation, *Clim. Past*, *7*(1), 319–338, doi:10.5194/cp-7-319-2011.

Breiman, L., and J. H. Friedman (1985), Estimating optimal transformations for multiple regression and correlation, *J. Am. Stat. Assoc.*, *80*(391), 580–598.

Burke, A., O. Marchal, L. I. Bradtmiller, J. F. McManus, and R. François (2011), Application of an inverse method to interpret ^{231}Pa/^{230}Th observations from marine sediments, *Paleoceanography*, *26*, PA1212, doi:10.1029/2010PA002022.

Butzin, M., M. Prange, and G. Lohmann (2005), Radiocarbon simulations for the glacial ocean: The effects of wind stress, Southern Ocean sea ice and Heinrich events, *Earth Planet. Sci. Lett.*, *235*(1–2), 45–61.

Carter, P., D. Vance, C. Hillenbrand, J. Smith, and D. Shoosmith (2012), The neodymium isotopic composition of waters masses in the eastern Pacific sector of the Southern Ocean, *Geochim. Cosmochim. Acta*, *79*(0), 41–59, doi:10.1016/j.gca.2011.11.034.

Chikamoto, M. O., L. Menviel, A. Abe-Ouchi, R. Ohgaito, A. Timmermann, Y. Okazaki, N. Harada, A. Oka, and A. Mouchet (2012), Variability in North Pacific intermediate and deep water ventilation during Heinrich events in two coupled climate models, *Deep Sea Res., Part II*, *61–64*, 114–126, doi:10.1016/j.dsr2.2011.12.002.

Colin, C., N. Frank, K. Copard, and E. Douville (2010), Neodymium isotopic composition of deep-sea corals from the NE Atlantic: Implications for past hydrological changes during the Holocene, *Quat. Sci. Rev.*, *29*(19–20), 2509–2517, doi:10.1016/j.quascirev.2010.05.012.

Crocket, K., D. Vance, M. Gutjahr, G. Foster, and D. Richards (2011), Persistent Nordic deep-water overflow to the glacial North Atlantic, *Geology*, *39*, 515–518, doi:10.1130/G31677.1.

Curry, W., and D. Oppo (2005), Glacial water mass geometry and the distribution of $\delta^{13}C$ of $\sum CO_2$ in the western Atlantic Ocean, *Paleoceanography*, *20*, PA1017, doi:10.1029/2004PA001021.

Elderfield, H., P. Ferretti, M. Greaves, S. Crowhurst, I. N. McCave, D. Hodell, and A. M. Piotrowski (2012), Evolution of ocean temperature and ice volume through the mid-pleistocene climate transition, *Science*, *337*, 704–709.

Foster, G. L., D. Vance, and J. Prytulak (2007), No change in the neodymium isotope composition of deep water exported from the North Atlantic on glacial-interglacial time scales, *Geology*, *35*(1), 37–40.

Frank, M. (2002), Radiogenic isotopes: Tracers of past ocean circulation and erosional input, *Rev. Geophys.*, *40*(1), 1–38, doi:10.1029/2000RG000094.

Friedrich, T., and A. Oschlies (2009a), Neural-network based estimates of North Atlantic surface pCO_2 from satellite data—A methodological study, *J. Geophys. Res.*, *114*, C03020, doi:10.1029/2007JC004646.

Friedrich, T., and A. Oschlies (2009b), Basinscale pCO_2 maps estimated from ARGO float data—A model study, *J. Geophys. Res.*, *114*, C10012, doi:10.1029/2009JC005322.

Friedrich, T., and A. Timmermann (2012), Millennial-scale glacial meltwater pulses and their effect on the spatiotemporal benthic $\delta^{18}O$ variability, *Paleoceanography*, *27*, PA3215, doi:10.1029/2012PA002330.

Goldstein, S., and S. Hemming (2003), Long lived isotopic tracers in oceanography, paleoceanography and ice-sheet dynamics, in *Treatise on Geochemistry*, vol. 6, edited by H. D. Holland and K. K. Turekian, pp. 453–489, Elsevier, New York.

Goosse, H., et al. (2010), Description of the Earth system model of intermediate complexity LOVECLIM version 1.2, *Geosci. Model Dev.*, *3*, 603–633.

Gutjahr, M., and J. Lippold (2011), Early arrival of southern source water in the deep North Atlantic prior to Heinrich event 2, *Paleoceanography*, *26*, PA2101, doi:10.1029/2011PA002114.

Gutjahr, M., M. Frank, C. Stirling, L. Keigwin, and A. Halliday (2008), Tracing the Nd isotope evolution of North Atlantic deep and intermediate waters in the western North Atlantic since the Last Glacial Maximum from blake ridge sediments, *Earth Planet. Sci. Lett.*, *266*(1–2), 61–77, doi:10.1016/j.epsl.2007.10.037.

Gutjahr, M., B. A. Hoogakker, M. Frank, and I. N. McCave (2010), Changes in North Atlantic deep water strength and bottom water masses during marine isotope stage 3 (45–35ka B.P.), *Quat. Sci. Rev.*, *29*(19–20), 2451–2461, doi:10.1016/j.quascirev.2010.02.024.

Hemming, S. R. (2004), Heinrich events: Massive late Pleistocene detritus layers of the North Atlantic and their global climate imprint, *Rev. Geophys.*, *42*(1), RG1005, doi:10.1029/2003RG000128.

Hesse, T., M. Butzin, T. Bickert, and G. Lohmann (2011), A model-data comparison of ^{13}C in the glacial Atlantic Ocean, *Paleoceanography*, *26*, PA3220, doi:10.1029/2010PA002085.

Hoffmann, S. S., J. F. McManus, W. B. Curry, and L. S. Brown-Leger (2013), Persistent export of ^{231}Pa from the deep central Arctic Ocean over the past 35,000 years, *Nature*, *497*, 603–607.

Horikawa, K., Y. Asahara, K. Yamamoto, and Y. Okazaki (2010), Intermediate water formation in the Bering Sea during glacial periods: Evidence from neodymium isotope ratios, *Geology*, *38*(5), 435–438.

Huang, K.-F., D. W. Oppo, and W. B. Curry (2014), Decreased influence of Antarctic intermediate water in the tropical Atlantic during North Atlantic cold events, *Earth Planet. Sci. Lett.*, *389*, 200–208, doi:10.1016/j.epsl.2013.12.037.

Itambi, A. C., T. von Dobeneck, S. Mulitza, T. Bickert, and D. Heslop (2009), Millennial-scale northwest African droughts related to Heinrich events and Dansgaard-Oeschger cycles: Evidence in marine sediments from offshore Senegal, *Paleoceanography*, *24*, PA1205, doi:10.1029/2007PA001570.

Jacobsen, S. B., and G. Wasserburg (1980), Sm-Nd isotopic evolution of chondrites, *Earth Planet. Sci. Lett.*, *50*(1), 139–155, doi:10.1016/0012-821X(80)90125-9.

Jeandel, C., T. Arsouze, F. Lacan, P. Téchiné, and J.-C. Dutay (2007), Isotopic Nd compositions and concentrations of the lithogenic inputs into the ocean: A compilation, with an emphasis on the margins, *Chem. Geol.*, *239*(1–2), 156–164, doi:10.1016/j.chemgeo.2006.11.013.

Johnson, H. L., and D. P. Marshall (2002), A theory for the surface Atlantic response to thermohaline variability, *J. Phys. Oceanogr.*, *32*, 1121–1132.

Jones, K. M., S. P. Khatiwala, S. L. Goldstein, S. R. Hemming, and T. van de Flierdt (2008), Modeling the distribution of Nd isotopes in the oceans using an ocean general circulation model, *Earth Planet. Sci. Lett.*, *272*(3–4), 610–619, doi:10.1016/j.epsl.2008.05.027.

Kawase, M. (1987), Establishment of deep ocean circulation driven by deep water production, *J. Phys. Oceanogr.*, *17*, 2294–2317.

©2014. American Geophysical Union. All Rights Reserved.

Kienast, M., S. S. Kienast, S. E. Calvert, T. I. Eglinton, G. Mollenhauer, R. François, and A. C. Mix (2006), Eastern Pacific cooling and Atlantic overturning circulation during the last deglaciation, *Nature*, *443*, 846–849.

Kienast, S. S., T. Friedrich, N. Dubois, P. S. Hill, A. Timmermann, A. C. Mix, and M. Kienast (2013), Near collapse of the meridional SST gradient in the eastern equatorial Pacific during Heinrich Stadial 1, *Paleoceanography*, *28*, 663–674, doi:10.1002/2013PA002499.

Kohonen, T. (1982), Self-organized formation of topologically correct feature maps, *Biol. Cybern.*, *43*, 59–69.

Lacan, F., and C. Jeandel (2005), Neodymium isotopes as a new tool for quantifying exchange fluxes at the continent—Ocean interface, *Earth Planet. Sci. Lett.*, *232*(3–4), 245–257, doi:10.1016/j.epsl.2005.01.004.

Lacan, F., K. Tachikawa, and C. Jeandel (2012), Neodymium isotopic composition of the oceans: A compilation of seawater data, *Chem. Geol.*, *300*, 177–184, doi:10.1016/j.chemgeo.2012.01.019.

Lippold, J., Y. Luo, R. Francois, S. E. Allen, J. Gherardi, S. Pichat, B. Hickey, and H. Schulz (2012), Strength and geometry of the glacial Atlantic meridional overturning circulation, *Nat. Geosci.*, *5*(11), 813–816.

Lund, D. C., J. F. Adkins, and R. Ferrari (2011), Abyssal Atlantic circulation during the Last Glacial Maximum: Constraining the ratio between transport and vertical mixing, *Paleoceanography*, *26*, PA1213, doi:10.1029/2010PA001938.

Lynch-Stieglitz, J., et al. (2007), Atlantic meridional overturning circulation during the Last Glacial Maximum, *Science*, *316*, 66–69.

Marchal, O., R. François, T. F. Stocker, and F. Joos (2000), Ocean thermohaline circulation and sedimentary $^{231}Pa/^{230}Th$ ratio, *Paleoceanography*, *15*, 625–641.

McManus, J. F., R. Francois, J. M. Gherardi, L. D. Keigwin, and S. Brown-Leger (2004), Collapse and rapid resumption of Atlantic meridional circulation linked to deglacial climate changes, *Nature*, *428*, 834–837.

Menviel, L., A. Timmermann, A. Mouchet, and O. Timm (2008), Meridional reogranization of marine and terrestrial productivity during Heinrich events, *Paleoceanography*, *23*, PA1203, doi:10.1029/2007PA001445.

Menviel, L., A. Timmermann, O. Elison Timm, and A. Mouchet (2010), Climate and biogeochemical response to a rapid melting of the West Antarctic Ice Sheet during interglacials and implications for future climate, *Paleoceanography*, *25*, PA4231, doi:10.1029/2009PA001892.

Menviel, L., A. Timmermann, O. Elison Timm, and A. Mouchet (2011), Deconstructing the last glacial termination: The role of millennial and orbital-scale forcings, *Quat. Sci. Rev.*, *30*, 1155–1172.

Menviel, L., A. Timmermann, O. E. Timm, A. Mouchet, A. Abe-Ouchi, M. Chikamoto, N. Harada, R. Ohgaito, and Y. Okazaki (2012), Removing the North Pacific halocline: Effects on global climate, ocean circulation and the carbon cycle, *Deep Sea Res. Part II*, *6–64*, 106–113, doi:10.1016/j.dsr2.2011.03.005.

Moreno, A., I. Cacho, M. Canals, M. Prins, M.-F. Sánchez-Goñi, J. Grimalt, and G. Weltje (2002), Saharan dust transport and high-latitude glacial climatic variability: The Alboran Sea record, *Quat. Res.*, *58*, 318–328.

Negre, C., R. Zahn, A. L. Thomas, P. Masqué, G. M. Henderson, G. Martínez-Méndez, I. R. Hall, and J. L. Mas (2010), Reversed flow of Atlantic deep water during the Last Glacial Maximum, *Nature*, *468*, 84–88, doi:10.1038/nature09508.

Noble, T. L., A. M. Piotrowski, and I. McCave (2013), Neodymium isotopic composition of intermediate and deep waters interglacial southwest Pacific, *Earth Planet. Sci. Lett.*, *384*, 27–36.

Okazaki, Y., A. Timmermann, L. Menviel, N. Harada, A. Abe-Ouchi, M. O. Chikamoto, A. Mouchet, and H. Asahi (2010), Deep water formation in the North Pacific during the last glacial termination, *Science*, *329*, 200–204.

Pahnke, K., and R. Zahn (2005), Southern Hemisphere water mass conversion linked with North Atlantic climate variability, *Science*, *307*, 1741–1746.

Pahnke, K., J. P. Sachs, L. Keigwin, A. Timmermann, and S.-P. Xie (2007), Eastern tropical Pacific hydrologic changes during the past 27,000 years from D/H ratios in alkenones, *Paleoceanography*, *22*, PA4214, doi:10.1029/2007PA001468.

Pahnke, K., S. L. Goldstein, and S. R. Hemming (2008), Abrupt changes in Antarctic Intermediate Water circulation over the past 25,000 years, *Nat. Geosci.*, *1*, 870–874.

Pena, L., S. L. Goldstein, S. R. Hemming, K. M. Jones, E. Calvo, C. Pelejero, and I. Cacho (2013), Rapid changes in meridional advection of Southern Ocean intermediate waters to the tropical Pacific during the last 30kyr, *Earth Planet. Sci. Lett.*, *368*, 20–32.

Piepgras, D. J., and G. J. Wasserburg (1982), Isotopic Composition of Neodymium in Waters from the Drake Passage, *Science*, *217*(4556), 207–214.

Piotrowski, A., A. Galy, J. Nicholl, N. Roberts, D. Wilson, J. Clegg, and J. Yu (2012), Reconstructing deglacial North and South Atlantic deep water sourcing using foraminiferal Nd isotopes, *Earth Planet. Sci. Lett.*, *357–358*, 289–297, doi:10.1016/j.epsl.2012.09.036.

Piotrowski, A. M., S. L. Goldstein, S. R. Hemming, and R. G. Fairbanks (2004), Intensification and variability of ocean thermohaline circulation through the last deglaciation, *Earth Planet. Sci. Lett.*, *225*(1–2), 205–220, doi:10.1016/j.epsl.2004.06.002.

Piotrowski, A. M., S. L. Goldstein, S. R. Hemming, and R. G. Fairbanks (2005), Temporal relationships of carbon cycling and ocean circulation at glacial boundaries, *Science*, *307*, 1933–1938.

Piotrowski, A. M., S. L. Goldstein, S. R. Hemming, R. G. Fairbanks, and D. R. Zylberberg (2008), Oscillating glacial northern and southern deep water formation from combined neodymium and carbon isotopes, *Earth Planet. Sci. Lett.*, *272*(1–2), 394–405, doi:10.1016/j.epsl.2008.05.011.

Piotrowski, A. M., V. K. Banakar, A. E. Scrivner, H. Elderfield, A. Galy, and A. Dennis (2009), Indian Ocean circulation and productivity during the last glacial cycle, *Earth Planet. Sci. Lett.*, *285*(–2), 179–189, doi:10.1016/j.epsl.2009.06.007.

Rempfer, J., T. F. Stocker, F. Joos, J.-C. Dutay, and M. Siddall (2011), Modelling Nd-isotopes with a coarse resolution ocean circulation model: Sensitivities to model parameters and source/sink distributions, *Geochim. Cosmochim. Acta*, *75*(20), 5927–5950, doi:10.1016/j.gca.2011.07.044.

Rempfer, J., T. F. Stocker, F. Joos, and J. Dutay (2012a), On the relationship between Nd isotopic composition and ocean overturning circulation in idealized freshwater discharge events, *Paleoceanography*, *27*, PA3211, doi:10.1029/2012PA002312.

Rempfer, J., T. F. Stocker, F. Joos, and J. Dutay (2012b), Sensitivity of Nd isotopic composition in seawater to changes in Nd sources and paleoceanographic implications, *J. Geophys. Res.*, *117*, C12010, doi:10.1029/2012JC008161.

Ritz, . P., T. F. Stocker, J. O. Grimalt, L. Menviel, and A. Timmermann (2013), Estimated strength of the Atlantic overturning circulation during the last deglaciation, *Nat. Geosci.*, *6*, 208–212.

Roberts, N. L., A. M. Piotrowski, J. F. McManus, and L. D. Keigwin (2010), Synchronous deglacial overturning and water mass source changes, *Science*, *327*, 75–78.

Robinson, L. F., and T. van de Flierdt (2009), Southern Ocean evidence for reduced export of North Atlantic Deep Water during Heinrich event 1, *Geology*, *37*(3), 195–198.

Roy, M., T. van de Flierdt, S. R. Hemming, and S. L. Goldstein (2007), $^{40}Ar/^{39}Ar$ ages of hornblende grains and bulk Sm/Nd isotopes of circum-Antarctic glacio-marine sediments: Implications for sediment provenance in the Southern Ocean, *Chem. Geol.*, *244*, 507–519.

©2014. American Geophysical Union. All Rights Reserved.

Rutberg, R. L., S. R. Hemming, and S. L. Goldstein (2000), Reduced North Atlantic Deep Water flux to the glacial Southern Ocean inferred from neodymium isotope ratios, *Nature*, *405*, 935–938.

Siddall, M., S. Khatiwala, T. van de Flierdt, K. Jones, S. L. Goldstein, S. Hemming, and R. F. Anderson (2008), Towards explaining the Nd paradox using reversible scavenging in an ocean general circulation model, *Earth Planet. Sci. Lett.*, *274*(3–4), 448–461, doi:10.1016/j.epsl.2008.07.044.

Skinner, L., A. Scrivner, D. Vance, S. Barker, S. Fallon, and C. Waelbroeck (2013), North Atlantic versus Southern Ocean contributions to a deglacial surge in deep ocean ventilation, *Geology*, *41*, 667–670, doi:10.1130/G34133.1.

Skinner, L. C., S. Fallon, C. Waelbroeck, E. Michel, and S. Barker (2010), Ventilation of the deep Southern Ocean and deglacial CO_2 rise, *Science*, *328*, 1147–1151.

Stichel, T., M. Frank, J. Rickli, and B. A. Haley (2012), The hafnium and neodymium isotope composition of seawater in the Atlantic sector of the Southern Ocean, *Earth Planet. Sci. Lett.*, *317–318*, 282–294, doi:10.1016/j.epsl.2011.11.025.

Stocker, T. F., A. Timmermann, M. Renold, and O. Timm (2007), Effects of salt compensation on the climate model response in simulations of large changes of the Atlantic meridional overturning circulation, *J. Clim.*, *20*, 5912–5928.

Tachikawa, K., A. M. Piotrowski, and G. Bayon (2014), Neodymium associated with foraminiferal carbonate as a recorder of seawater isotopic signatures, *Quat. Sci. Rev.*, *88*, 1–13.

Thomas, E., L. Booth, M. . Maslins, and N. J. Shackleton (1995), Northeastern Atlantic benthic foraminifera during the last 45,000 years: Changes in productivity seen from the bottom up, *Paleoceanography*, *10*(3), 545–562.

Timmermann, A., H. U. Voss, and R. Pasmanter (2001), Empirical dynamical system modeling of ENSO using nonlinear inverse techniques, *J. Phys. Oceanogr.*, *31*, 1579–1598.

Tjallingii, R., M. Claussen, J.-B. Stuut, J. Fohlmeister, A. Jahn, T. Bickert, F. Lamy, and U. Röhl (2008), Coherent high- and low-latitude forcing of the Northwest African humidity, *Nat. Geosci.*, *289*, 670–675, doi:10.1038/ngeo289.

von Blanckenburg, F. (1999), Paleoceanography—Tracing past ocean circulation?, *Science*, *286*, 1862–1863.

Weaver, A., O. Saenko, P. Clark, and J. Mirtovica (2003), Meltwater pulse 1A from Antarctica as a trigger of the Bølling-Allerød warm interval, *Science*, *299*, 1709–1713.

Weber, M. E., et al. (2014), Millennial-scale variability of the Antarctic Ice Sheet throughout the last deglaciation, *Nature*, *510*, 134–138, doi:10.1038/nature13397.

Wilson, D. J., A. M. Piotrowski, A. Galy, and I. N. McCave (2012), A boundary exchange influence on deglacial neodymium isotope records from the deep western Indian Ocean, *Earth Planet. Sci. Lett.*, *341–344*, 35–47.

Wilson, D. J., A. M. Piotrowski, A. Galy, and J. A. Clegg (2013), Reactivity of neodymium carriers in deep sea sediments: Implications for boundary exchange and paleoceanography, *Geochim. Cosmochim. Acta*, *109*, 197–221.

Xie, R. C., F. Marcantonio, and M. W. Schmidt (2012), Deglacial variability of Antarctic intermediate water penetration into the North Atlantic from authigenic neodymium isotope ratios, *Paleoceanography*, *27*, PA3221, doi:10.1029/2012PA002337.

Xie, R. C., F. Marcantonio, and M. W. Schmidt (2014), Reconstruction of intermediate water circulation in the tropical North Atlantic during the past 22,000 years, *Geochim. Cosmochim. Acta*, *140*, 455–467, doi:10.1016/j.gca.2014.05.041.

Xie, S.-P., Y. Okumura, T. Miyama, and A. Timmermann (2008), Influences of Atlantic climate change on the tropical Pacific via the Central American Isthmus, *J. Clim.*, *21*(15), 3914–3928.

Yu, E.-F., R. François, and M. P. Bacon (1996), Similar rates of modern and last-glacial ocean thermohaline circulation inferred from radiochemical data, *Nature*, *379*, 689–694.

©2014. American Geophysical Union. All Rights Reserved.